IMPEDANCE BASED APTASENSOR FOR THE DETECTION OF *MYCOBACTERIUM TUBERCULOSIS* SECRETED PROTEIN MPT64

Marzhan Sypabekova

A thesis submitted in partial fulfilment of the requirements of Nazarbayev University for the degree of Doctor of Philosophy in Science, Engineering and Technology

June 2019

Abstract

Tuberculosis (TB) detection remains a significant healthcare issue in the developing world owing to a number of challenges. Current diagnostics are based on microbiological culturing, sputum smear microscopy, and nucleic acid amplification tests. These methods suffer from limitations such as batch to batch variations, frequent contaminations, low sensitivity, and the

requirement for special facilities, expensive devises, reagents, and trained personnel.

This thesis describes the development of the sensitive oligonucleotide-based aptasensor for the detection of TB biomarker MPT64 protein. The dissertation investigates the selection and use of ssDNA aptamers to detect MPT64 using the electrochemical impedance spectroscopy (EIS). Aptamers serve as bio-recognition elements in this study, and they have numerous advantages including cheap cost, ease of modification and long shelf life. The combination of aptamers with the EIS offers sensitive detection since the change in EIS signal can be recorded as the result of analyte binding event based not only on molecular interaction level but also on electron transfer levels.

As the result 17 unique aptamer sequences were purified and analyzed. One aptamer with dissociation equilibrium constant K_D of 8.92 nM was selected and the surface chemistry was optimized based on ssDNA aptamer modified with a long linker and 6-mercaptohexanol as a co-adsorbent at 1/100 ratio. The selected aptamer was further immobilized on an interdigitated microelectrode and connected to a portable potentiostat. The detection time for aptasensor was found to be 15 min. The aptasensor was tested on clinical samples and showed increased binding to TB (+) samples as compared to TB (-) samples. The integration of the aptasensor with the in house built fluidic chamber and liquid flow rate within chamber was also investigated.

The work in this thesis is significant as it can contribute to the diagnosis of TB (non-invasive), monitoring of anti-TB treatment in infected people and hence to socio-economic development of the country. It is the first portable aptasensor which is developed using aptamers and EIS as a detection technique that can provide fast clinical sample analysis (reduced from 3 h to 15 min) as well as elimination of using of extra reagents, equipment, and personnel.

Table of contents

List of tables

List of Figures

Figure 2.3 A typical graph of an AC signal of the applied voltage and obtained current response during the impedance measurement.

Figure 2.4 A schematic representation of an electron transfer promotion and inhibition in Faradaic mode on a receptor modified electrode with (right) and without (left) target analyte.

Figure 2.5 Schematic overview of an electrical double layer of a receptor modified electrode electrolyte interface.

Figure 2.6 (a) A typical Nyquist plot with a semicircle region followed by a straight line. The semicircle part indicates a charge-transfer limited process in the high-frequency range and the linear part indicates a mass-transfer limited process in the low-frequency range. The R_s (solution resistance) and R_{ct} (charge transfer resistance) values could be determined from the Nyquist plot. The R_{ct} is an electrical parameter in analyzing the impedance signal change for the detection of protein; (b) Randles equivalent circuit, where R_s is not affected by the binding process, R_{ct}, Z_w Warburg impedance, and C_{DL} the double layer capacitance.

Figure 2.7 Schematic structure of the IDE. Two individually addressable interdigitated comb like electrode structures made of metal deposited on a substrate.

Figure 3.1 A schematic representation of principles and concepts of selection and characterization of MPT64 aptamers using SELEX, dot blot, cloning, sequencing, and ELONA techniques.

Figure 3.2 (a) 6% TBE-PAGE analysis of PCR products from cycle 6 of in vitro selection of aptamers against target MPT64 by SELEX method stained with SYBR Green I: Lane 1. PCR product of SELEX cycle 6, Lane 2. 25 bp DNA ladder; (b) Dot blot analysis of affinity binding between aptamer pools from the SELEX cycle 5 and target MPT64, and two controls; (c) Affinity evaluation of the ssDNA aptamer sequence (4) using dot blot analysis method. “+” control E. coli antibodies labelled with biotin (diluted at 1:500), “-” control - deionized water.

Figure 3.3 The binding affinity of selected ssDNA aptamers to proteins MPT64, ESAT-6, CFP 10. Binding of biotinylated ssDNA aptamers to the target MPT64, and non-target ESAT-6 and CFP-10 was determined by an ELONA assay. Binding of the ssDNA aptamers to ESAT-6 and CFP-10 is shown for comparative purposes. (a) Individual aptamer sequences (1-17) (500 nM) were incubated in wells coated with target MPT64, and non-target ESAT-6 and CFP-10. Aptamers (17) are shown in circles. All data are shown in the form of Mean±SEM (n=6). (b) ELONA analysis of the relative binding abilities of individual aptamer sequences (1-17). (c) Binding of the aptamer sequence (17) to the target MPT64. All data are shown in the form of Mean±SEM (n=3).

Figure 3.4 The binding affinity of selected ssDNA aptamers to proteins MPT64, ESAT-6, CFP 10. Binding of biotinylated ssDNA aptamer candidates to target MPT64, and to non-target ESAT-6 and CFP-10 was determined by ELONA. Binding of ssDNA aptamers to non-target ESAT-6 and CFP-10 is shown for comparative purposes. Aptamer sequences (1-17) (500 nM) were incubated in wells coated with proteins MPT64, ESAT-6 and CFP-10. All data are shown in the form of Mean±SEM (n=6).

Figure 3.5 (a) Schematic representation of SPR. P-polarised light is directed to the high refractive index prism (in contact with the streptavidin coated SA chip), on which the biotinylated aptamer is attached. The output signal in the form of the reflected light is then represented as resonant unit variations vs time upon protein (MPT64) binding. (b) An overlay of the SPR signals from the interaction between the target MPT64 and aptamer (17). In each case, MPT64 was injected over immobilized aptamer (17) with an initial concentration of 2.5, followed by 5, 10, 20, and 40 μg/ml.

Figure 3.6 Detection of MPT64 antigens in sputum samples. (a) ELONA based assay for the detection of MPT64 antigens in TB infected and TB (-) using aptamer sequences (16) and (17); (b, c) The ROC curve of aptamer sequences (17) and (16), respectively, based on ELONA.

Figure 4.1 An aptasensor surface modification based on different chemistries applied onto the

gold surface of the electrode; (a) short linker DNA aptamer/MCH; (b) long linker DNA aptamer/EG; (c) long linker DNA aptamer/MCH.

Figure 4.2 Target MPT64 detection using BioFET. (a) A schematic representation of BioFET set-up; (b) A typical I_D/V_{GS} characteristic curve for an electrode before (solid line) and after (dashed line) MPT64 binding event based on a long linker aptamer/MCH complex; (c) VGS changes on the surface of the electrode upon incubation with different MPT64 concentrations in SELEX buffer based on a short linker aptamer/MCH (1/100 ratio), long linker aptamer/EG (1/100 ratio), and long linker aptamer/MCH (1/100 ratio). All measurements were recorded on three separate electrodes.

Figure 4.3 R_{ct} change for the electrode surface treated with a short linker-DNA aptamer/MCH and long linker DNA aptamer/MCH at a ratio of 1/100 followed by target incubation and measurement (in SELEX measurement buffer (50 mM Tris-HCl; 25 mM NaCl; 5 mM $MgCl_2$; pH 7.5) containing 2 mM ferro/ferricyanide $[Fe(CN)_6]^{3-/4-}$redox couple. Error bars show the mean and spread for at least three measurements from separate electrodes.

Figure 4.4 An example of non-Faradaic EIS measurement of the electrode modified long linker DNA aptamer/EG based surface chemistry upon MPT64 binding. Inset: original data.

Figure 4.5 Contact angle measured on different steps of aptasensor fabrication using aptamer/MCH ratio at 1/100. Error bars show the mean and spread for at least three measurements from separate electrodes.

Figure 4.6 Contact angle measurement images corresponding to (a) bare gold; (b) MCH; (c) MCH/aptamer; (d) MCH/aptamer MPT64; (e) MCH/aptamer HSA.

Figure 4.7 a) Charge flow graph for the gold electrode functionalized with the long linker DNA aptamer/MCH at a 1/100 ratio in a solution of 10 mM Tris-HCl pH 7.4 with and without $Ru(NH_3)_6^{3+.}$ The potential was stepped from -300 to -800 mV versus Hg/Hg_2SO_4 reference electrode 500 ms; (b) Chronocoulometric response curves for the gold electrode functionalized

with the long linker DNA aptamer/MCH at a 1/100 ratio.

Figure 4.8 (a) Aptamer molecule density distribution on the electrode surface vs. aptamer/MCH molar fraction in solution. The measurements were based on the resulting charge change in the absence and presence of 100 μM hexaamimmeruthenium (III) chloride ($Ru(NH_3)_6^{3+}$) in 10 mM Tris-HCl pH 7.4. (b) Change in charge transfer resistance (R_{ct}) of an electrode measured in 30 min intervals at different MPT64 concentrations binding at different aptamer/MCH ratios. The measurements were recorded in SELEX buffer containing 2 mM ferro/ferricyanide $[Fe(CN)_6]^{3-/4-}$ redox couple. Error bars show the mean and spread for at least three measurements from separate electrodes.

Figure 4.9 (a) A schematic overview of the gold electrode surface modification with a long linker DNA aptamer/MCH followed by target MPT64 capturing event on the functionalized surface of the gold electrode; (b) A representative Nyquist plot (-Z'' vs. Z') for the blank electrode (circle, black), for electrode with immobilized aptamer/MCH before (triangle, blue and triangle, red) and after (rectangle, green) interaction with MPT64 protein for 30 min. Measured data were shown as symbols with calculated fit to the equivalent circuit as dashed lines. (c) A concentration-dependent curve for different MPT64 concentrations using a long linker DNA aptamer/MCH at a ratio of 1/100 relative to blank measurements from the EIS signal measured in SELEX buffer; Inset: A linear correlation curve with regression equation between R_{ct} change value and the target protein from 1 nM to 50 nM; (d) a Nyquist plot for different MPT64 concentrations (in nM) using a long linker DNA aptamer/MCH in a ratio of 1/100 (experimentally obtained values shown as dots; fitted values shown as dashed lines).

Figure 4.10 Specificity study of the electrochemical aptasensor for the target MPT64 detection along with HSA, CEA, and PSA detection at different concentrations based on long linker DNA aptamer/MCH surface chemistry at an optimized ratio of 1/100. Change in charge transfer resistance (R_{ct}) of an electrode measured in 30 min intervals in SELEX buffer containing 2 mM

ferro/ferricyanide $[Fe(CN)_6]^{3-/4-}$ redox couple. Error bars show the mean and spread for at least three measurements from separate electrodes.

Figure 4.11 Change in charge transfer resistance (R_{ct}) of an electrode measured in 30 min intervals at different MPT64 concentrations at 1/100 long linker aptamer/MCH ratio. Data was recorded in buffers containing 2 mM ferro/ferricyanide $[Fe(CN)_6]^{3-/4-}$redox couple: (a) SELEX buffer; (b) 10 x diluted SELEX measurement buffer; (c) 10 mM PBS pH 7.4; (d) 1 mM PBS pH 7.4. Error bars show the mean and spread for at least three measurements from separate electrodes.

Figure 4.12 (a) A representative Nyquist plot (-Z'' vs. Z') for an electrode with immobilized aptamer/MCH in buffer (triangle, blue) and in serum (circle, black). Measured data were shown as symbols with the calculated fit (Randles equivalent circuit) to the equivalent circuit as dashed lines. (b) A change in the charge transfer resistance (R_{ct}) of an electrode measured in 30 min intervals at different MPT64 concentrations 1/100 diluted serum samples using EIS. The measurements were taken in SELEX measurement buffer containing 2 mM ferro/ferricyanide $[Fe(CN)_6]^{3-/4-}$redox couple. Black squares represent values obtained from incubation with different MPT64 concentrations diluted in serum. Dashed tread line represents repetitive measurements of serum sample without MPT64. Error bars show the mean and spread for at least three measurements from separate electrodes.

Figure 4.13 Change in charge transfer resistance (R_{ct}) of an electrode measured in 30 min intervals at different MPT64 concentrations spiked 1/100 diluted serum samples and SELEX buffer using EIS. The aptamer/MCH ratio was at 1/100. Error bars show the mean and spread for at least three measurements from separate electrodes.

Figure 4.15 Change in charge transfer resistance (R_{ct}) of an electrode measured in 30 min intervals at different MPT64 concentrations spiked 1/10 diluted serum samples using EIS. Black dots represent values obtained from incubation with different MPT64 concentrations diluted in serum. The aptamer/MCH ratio was at a 1/100 ratio. The dashed line represents the tread line for repetitive measurements of serum samples without MPT64. Error bars show the mean and spread for at least three measurements from separate electrodes.

Figure 5.1 The experimental set-up comprising a PC, portable potensiostat, electrodes (IDE,

CE, RE) imbedded in a chamber containing 2 mM ferro/ferricyanide $[Fe(CN)_6]^{3-/4-}$ redox couple (potassium hexacyanoferrate II/III) dissolved in SELEX buffer(50 mM Tris-HCl; 25 mM NaCl; 5 mM $MgCl_2$; pH 7.5).

Figure 5.2 (a) Typical impedance spectra of an IDE electrode before and after cleaning, after an aptamer/MCH immobilization step and after MPT64 binding. The measurements were recorded in SELEX buffer (50 mM Tris-HCl; 25 mM NaCl; 5 mM $MgCl_2$; pH 7.5) containing 2 mM ferro/ferricyanide $[Fe(CN)_6]^{3-/4-}$ redox couple; (b) IDE (I) drawing and (II) IDE image taken by camera. The region indicated in red (the part of the active area) magnified using the microscope. The active area is composed of two interdigitated electrodes with two connection tracks, all made of gold, on a glass substrate with bands/gaps at 5 μm with dimensions L 22.8 × W 7.6 × H 0.7 mm. Electrode consisted of 250 × 2 digits with the digit length of 6,760 μm.

Figure 5.3 (a) An optimization study of the incubation time (5, 10, 15, and 20 min) required for 1 fM MPT64 detection with the use of the electrochemical aptasensor and modified IDE. The IDE surface was modified by aptamer/MCH complex at a ratio of 1/100, and the EIS signal was measured in SELEX buffer; (b) A specificity study of the electrochemical aptasensor for the target MPT64 detection along with CFP-10 and ESAT-6 at different concentrations based on the DNA aptamer/MCH surface chemistry at an optimized ratio of 1/100. Presented change in R_{ct} of the IDE was measured in 15 min intervals in SELEX buffer containing 2 mM ferro/ferricyanide $[Fe(CN)_6]^{3-/4-}$ redox couple.

Figure 5.4 (a) A concentration-dependent curve for different MPT64 concentrations using aptamer/MCH at a ratio of 1/100 relative to blank measurements from the EIS signal measured in SELEX buffer (50 mM Tris-HCl; 25 mM NaCl; 5 mM $MgCl_2$; pH 7.5); Inset: Randles equivalent circuit where R_s is the solution resistance, R_{ct} is the charge transfer resistance, C_{DL} is the constant phase element, and W is the Warburg element. Error bars show the mean and spread for at least three measurements. (b) an experimental Nyquist plot for different MPT64 concentrations using aptamer/MCH in a ratio of 1/100.

Figure 5.5 (a) AFM topographical micrographs in air of G-IDEAU 05 type gold plated IDE surfaces: (a, b) 2D and 3D micrographs of a bare IDE with the surface roughness of around 2.6

nm; (c, d) 2D and 3D micrographs of the IDE surface functionalized with the aptamer and average roughness of the surface of 4 - 4.5 nm high; (e, f) 2D and 3D micrographs of the aptamer functionalized IDE surface after incubation with a 1nM MPT64 and surface roughness of up to 20 nm high.

Figure 5.6 A representative micrograph of *M. tuberculosis* bacilli using an AFB staining technique. Staining of sputum sample from TB infected patient is presented. Red rod-shaped bacilli correspond to *M. tuberculosis*. Red arrows indicate some of the presumptive *M. tuberculosis.*

Figure 5.7 Evaluation of the aptasensor using clinical (a) serum and (c) sputum samples from infected TB (+) (active form) and TB (-) individuals and respective ROC curves (b,d).

Figure 6.1 The experimental set-up involving the fluidic device.

Figure 6.2 (a) Schematic and real view of the fluidic chamber with working area: height 195μm, radius 5.2 mm, volume 4.45 μL and with inlet and outlet flow system at an angle of 45^0; (b) Assembled fluidic device with a reference, counter and working electrodes. The bottom and the top part of the device was mounted via bolts and the working area was fixed using o-ring. The inlet and outlet tubes were positioned at 45° from the sensing surface. The inlet tube was connected to the pumping system which allowed the liquid flow at a specified flow rate. The red circle encloses the area where air bubbles formed during the course of the experiment; (c) Error message obtained during the impedance measurement: "Potentiostatic loop interrupted". On the background, a typical data for impedance vs. frequency measurement after protein binding.

Figure 6.3 Overall air volume fraction in the chamber *vs.* Filling-Time/Critical-Time at liquid flow rates of 15, 100, 500, and 1000 μL/min.

Figure 6.4 Assembled fluidic devise with reference, counter and working electrodes. The red arrow shows the area where air bubbles formed during the experiment at respective flow rates 1000, 500, 100, and 15 μl/min.

Figure 6.5 Impedance magnitude data for the detection of the target MPT64 at different concentrations of 1, 2, and 10 nM. The impedance magnitude increased with an increase of the target concentration.

Nomenclature

V Potential (V)

$\phi\phi_0$ amplitude of the signal

ω angular frequency (radians/seconds)

f Frequency (Hz)

$\phi\phi$ Phase shift

I Current (A)

Z Impedance (Ohm)

j imaginary number

R_{ct} charge transfer resistance

Z_w Warburg impedance (Ohm)

C_{DL} double layer capacitance (F)

Γ_{DNA} probe surface density (molecules/cm^2)

m the number of negatively charged phosphate groups on the probe DNA z charge on the redox molecule (C)

N_A Avogadro's constant (mol)

C' real part of the capacitance (F)

C'' imaginary part of the capacitance (F)

List of abbreviations

M. tuberculosis Mycobacterium tuberculosis

Ag-85 Antigen-85

AuNPs gold nanoparticles

BCG *Mycobacterium bovis* bacilli Calmette-Guérin Bio-FET

Biological Field Effect Transistor

CE counter electrode

CEA carcinoembryonic antigen

CFP-10 culture filtrate protein-10

CIS Commonwealth of Independent States EG triethylene glycol

mono-11-mercaptoundecyl ether EIS electrochemical impedance

spectroscopy ELISA enzyme linked immunosorbent assay

ESAT-6 early secreted antigenic target-6

HIV Human Immunodeficiency Virus

HSA human serum albumin

IDE Interdigitated microelectrode

IFN-g interferon-gamma

MCH 6-mercapto-1-hexanol

MDR-TB Multi Drug Resistant TB

MOSFET metal oxide semiconductor field-effect transistor MTBC

Mycobacterium tuberculosis Complex NAAT nucleic acid amplification

tests

NTM nontuberculous mycobacteria

PBMC peripheral blood mononuclear cells

PCR polymerase chain reaction

PNA peptide nucleic acid

PoC point of care monitoring

PSA prostate specific antigen

RD region of difference

RE reference electrode

List of abbreviations (continued)

RT-PCR reverse transcription polymerase chain reaction SAM

self-assembled monolayer

SELEX systematic evolution of ligands by exponential enrichment SPR surface plasmon resonance

ssDNA single stranded deoxyribonucleic acid

TB tuberculosis

WE working electrode

WHO World Health Organization

Acknowledgements

I would like to thank the Ministry of Education and Science of the Republic of Kazakhstan for the funding PhD program at Nazarbayev University. I would like to express my veneration and obligation and thanks to my supervisor Dr. Damira Kanayeva, co-supervisor Dr. Daniele Tosi and external supervisor Dr. Claude Nogues for supporting me in a friendly way every time I had a question. My supervisors have given me sustained guidance, patience, and encouragement throughout my research.

Moreover, I extend my sincerest thanks to all the members of Biosensor and Bioinstruments laboratory at Nazarbayev University for their comprehensive and most instructive collaborations, discussions, and support. I would like to thank British Council in Kazakhstan for giving me the opportunity to undertake part of my research in the UK, and my deepest gratitude to Dr. Pedro Estrela for his support and guidance throughout my time spent at the University of Bath.

I would also like to thank the anti-Tuberculosis dispensary chief doctor Anna Tsepke for an immense contribution to this thesis and all members of anti-Tuberculosis dispensary diagnostic laboratory for helping me in providing samples.

All my colleagues and friends Aliya Bekmurzayeva, Takhmina Auypova, Zhannat Ashikbayeva, Madina Shaimerdenova, Madina Zhelbuldina, Sanzhar Korganbayev, Ildar Bekniyazov, Pawan Jolly and Pavel Zhurauski for their constant support, help and shared moments.

Lastly, thanks to all the people who have helped me directly or indirectly for the day to day affairs.

Words seem inadequate to express the immense contribution of my husband, my daughters, my parents and other family members who have stood by me in all my endeavours and have always encouraged me.

Declaration

I declare that the research contained in this thesis, unless otherwise formally indicated within the text, is the original work of the author. The thesis has not been previously submitted to this or any other university for a degree and does not incorporate any material already submitted for a degree.

Chapter 1. Introduction

The work in this thesis aims at developing an oligonucleotide-based aptasensor for the detection of *Mycobacterium tuberculosis (M. tuberculosis)* secreted protein MPT64. In order to develop such a aptasensor, it is imperative to understand TB and the physiological processes

associated with it in patients. This Chapter describes the TB burden and its current diagnosis status. It also provides information on the aim of the dissertation as well as a set of objectives. Part of the work presented in this Chapter has been published in[1 2].

1.1 Tuberculosis burden

TB is one of the ancient infectious diseases and yet is the ninth leading cause of death worldwide[3]. The worldwide TB epidemic accounted for 10.4 million new cases and 480,000 new cases on multidrug-resistant TB with an estimated 1.4 million deaths in 2015[4]. In 2017, there were an estimated 1.3 million TB deaths among HIV (Human Immunodeficiency Virus) - negative people and an additional 300,000 deaths among HIV-positive people[5]. According to the latest report from World Health Organization (WHO) 10 million people developed TB in 2017 out of which 58% are men, 32% are women and 10% are children[5]. 87% of all TB cases were reported in 30 high TB burden countries (India, China, Philippines, and Pakistan etc.), 6% in WHO European region and 3% in WHO region of the Americas. The TB prevalent regions include South-East Asia Region (45%), the African Region (25%), the Western Pacific Region (17%)[3]. The continuing emergence of drug-resistant TB accounted for 558,000 cases in 2017 from which 457,576 accounted as multiple drug resistant TB (MDR-TB) with the most prevalent in countries such as India, China and countries of former Soviet Union[5] 23% of the world's population which is 1.7 billion people have latent TB infection and, hence, are at risk of developing active TB infection. In 1993, the WHO declared TB as a global emergency, and since 1997, WHO has been publishing a TB report annually to provide the up to date information on TB epidemic at global, regional, and country levels. Therefore, as recently reported by the End TB Strategy (WHO), there is still a need in improving the TB diagnosis quality, treatment, prevention and care[5].

The causative agent of TB is tubercule bacilli, *M. tuberculosis*. It has characteristic features which include slow growth, dormancy, complex cell envelope, intracellular pathogenesis, and genetic homogeneity[6]. The long generation time of *M. tuberculosis* (24 h) contributes to the

chronic nature of the disease, imposes lengthy treatment regimens and represents a formidable obstacle for researchers[7]. After an infection, *M. tuberculosis* may remain quiescent within infected tissue and may reflect metabolic shutdown resulting from the action of a cell-mediated

immune response that can contain but not eradicate the infection[7]. The cell envelope of *M. tuberculosis* is complex compromising a peptidoglycan layer, a layer with unusual lipids, glycolipids and polysaccharides[8]. Cell wall components include mycolic acids, mycocerosic acid, phenolthiocerol, lipoarabinomannan, and arabinogalactan[7]. The complex cell wall and envelope contribute to mycobacterial longevity, resistance, trigger inflammatory host reactions, and act in pathogenesis[7]. The major habitable niche for *M. tuberculosis* is human tissues and warm-blooded animals. The infection occurs when a susceptible person inhales airborne particles with *M. tuberculosis* and passes it to alveoli where they can be engulfed by alveolar macrophages. Depending on the cell-mediated immune response of the host, the bacilli can multiply in macrophages (active) or remain dormant (latent) for many years after initial infection. The mechanisms involved in life within the macrophage and nature of the virulence factors produced by the bacillus and their contribution to the disease is still under investigation. The latent form does not show tuberculosis symptoms, i.e. the growth of the bacteria inhibited by the host's immune system. The latent TB becomes active when the body's resistance lowers due to ageing, diabetes, HIV infection, and there is also an increased risk of acquiring TB for people with habits such as smoking and alcohol consumption[3]. The bacterium usually infects lungs (pulmonary, 90% of active cases) but can also affect other parts of the human body including (extrapulmonary, 10 - 20% of active cases) central nervous system, lymphatic system, genitourinary system, bones, and joints. When the active TB infects lungs, it involves symptoms such as prolonged coughing, chest pain, fever, chills, night sweats, loss of appetite, and weight loss.

As it was mentioned above, *M. tuberculosis* primarily infects alveolar macrophage eventually causing extensive lung inflammation and pathology[9]. The macrophage is a type of white blood cell that usually clears microorganisms by activating pathogen-recognition receptors through a lysosomal-trafficking pathway[10]. In macrophages, *M. tuberculosis* resides and replicates primarily in phagosomes, which are thought to be a nutritionally-constrained environment[11]. It is unclear how *M. tuberculosis* inhibits lysosomal-trafficking pathway, circumvent host defences, and cause disease by exploiting a specialized set of metabolic pathways. *M. tuberculosis* uses multiple sophisticated and precisely targeted mechanisms for inhibiting or

manipulating all of the known pathways for antigen presentation to T cells[12]. Studies indicate that the metabolism of host-derived carbon sources is critical for *M. tuberculosis* survival in

macrophages[13] [14]. Genetic manipulation of key genes involved in *M. tuberculosis* carbon metabolism also showed that the mutants associated with carbon metabolism fail to establish infection in macrophages[15]. By inhibiting host's innate immunity *M. tuberculosis* gains access to crucial intracellular nutrients such as acids and/or cholesterol, for energy production and maintain increased intracellular bacterial proliferation[12]. Infected macrophages in the lung usually attract lymphocytes and monocytes targeting the infected region via the production of chemokines and surface exposed bacterial antigens[16]. The immune cells surround the infected region and form granulomatous focal lesions composed of macrophage-derived giant cells where most bacteria killed. The resulting caseous tissue has the acidic pH, the low oxygen and the presence of toxic fatty acids[17]. Despite the hostile environment of the host, some bacilli may remain dormant but alive for many years (latent infection). The granulomas subsequently may heal, leaving small fibrous and calcified lesions. However, the bacilli can re-activate if the person's immune system becomes weakened. At this point, the granuloma centre can become liquefied by an unknown process and serves as a rich medium in which the revived bacteria can replicate in an uncontrolled manner[17] and further spread within the lungs (active pulmonary TB). The person with an active TB becomes infectious and has to be treated with an antibiotic from 6 months up to 2 years in an isolated environment. Mismanagement of the treatment and person-to-person transmission has resulted in developing antibiotic resistance in *M. tuberculosis*. *M. tuberculosis* has acquired resistance to different kinds of antibiotics increasing the number of MDR-TB. Drug-resistant TB is difficult and costly to treat extending the time a person needs to be treated, which sometimes is fatal[18]. Nowadays, Kazakhstan has one of the highest rates of morbidity and mortality from TB in Europe and the Commonwealth of Independent States (CIS). There are 26 severe TB cases per 100 thousand population registered in 2013. Moreover, Kazakhstan is one of the 24 countries in the Eurasian region, which has a high number of MDR[5].

1.2 Current TB detection techniques

Despite advances in diagnostics, a considerable proportion of the TB cases reported to WHO are still clinically diagnosed rather than bacteriologically confirmed[19]. For instance, only 57% of pulmonary TB cases reported to WHO were bacteriologically confirmed[3]. TB detection remains a significant healthcare issue in the developing world owing to a number of challenges.

First of all, mycobacterium is a slow-growing bacterium, and it takes 4-8 weeks to cultivate on traditional solid media and 10-14 days even with rapid liquid culture. Secondly, pulmonary TB presents low clinical symptoms early in the disease course, which leads to a delay in seeking professional care. Thirdly, active pulmonary TB may present low bacillary burden at the early stage, which often leads to low sensitivity for sputum smear microscopy, commonly used in the developing world. **Table 1.1** summarizes currently available TB detection methods including methods approved by WHO for routine use in tuberculosis antidispensaries and hospitals.

Microbiological culturing, sputum smear microscopy and Nucleic Acid Amplification (NAAT's) are routinely used diagnostics methods in TB dispensaries and hospitals. Microbiological culturing can detect a low number of *M. tuberculosis*; however, it suffers from batch to batch variations, frequent contamination and need for laboratories with a high level of isolation and security. In addition, since the bacterial growth is extremely slow, extended time is required for the result confirmation and validation. High rates of nontuberculous mycobacteria (NTM) found from positive cultures has been recorded which also sets a drawback in this technique[20]. Microscopy is another widely used technique for bacterial detection in resource limited countries. In this technique, sputum is smeared onto the microscope slide, stained and observed under the microscope. The sensitivity for this technique varies in HIV infected people[21]. The identification of *M. tuberculosis* and its differentiation from other mycobacterial species traditionally has been done by growth characteristics and biochemical reactions[22]. Biochemical tests are also slow and cumbersome in low resource settings[20]. NAATs are based on isolation, amplification and detection of *M. tuberculosis* gene segments. The technique has high sensitivity in patients identified positive for sputum smear microscopy but remains heterogeneous for a patient with negative sputum smear microscopy results[23]. The NAATs requires a set of expensive reagents, special laboratory conditions and trained personnel. There are also currently a number of serological tests for diagnosis of TB that are commercially available. However, compared to other diseases for which detection of antibodies or antigens in blood is used for diagnosis today, tuberculosis diagnosis with this method has not been successful so far. Most of them are rapid tests (based on lateral flow or flow-through) or microwell enzyme-linked immunosorbent assay (ELISA) tests[24]. Advantages of serological methods are convenience and simplicity in use, high negative predictive value and cost effectiveness. However, the clinical use of serology as a first-line screening tool does not provide enough sensitivity and specificity.

Detection of antibodies can often lead to false

positive results since antibodies against environmental mycobacteria are present in the sample thus cannot be used to distinguish infection with *M. tuberculosis* from nontuberculous mycobacteria (NTM). Moreover, serological methods in TB diagnosis cannot reliably distinguish active TB from latent TB[25-27].

Several attempts have been made for developing a biosensor for tuberculosis detection. Briefly, depending on the biomolecule that needs to be detected, two types of electrochemical biosensors have been developed: electrochemical immunosensors and DNA based biosensors. All DNA based electrochemical sensors for TB diagnosis were based on *M. tuberculosis* probe specificity. For instance, peptide nucleic acid (PNA) probes specific to 16 - 23s rRNA spacer region of *M. tuberculosis* has been covalently immobilized onto the polypyrrole-polyvinylsulphonate film[28]. The PNA probe was used for the hybridization detection with the complementary DNA sequence of *M. tuberculosis* with a detection limit of 2.5 pg/µL. Other study proposed dextrin coated gold nanoparticles (AuNPs) and amine-terminated magnetic particles (MPs) each functionalized with a different DNA probe that specifically hybridizes with opposite ends of a fragment within the *IS6110* gene, which is *M. tuberculosis* complex (MTC) specific. After hybridization, the formed complex (MP-target-AuNP) was magnetically separated from the solution, and AuNPs were electrochemically detected on a screen printed carbon electrode (SPCE) chip with a detection limit of 0.01 ng/µl[29]. Another study on graphene oxide–AuNPs that was served as a sensing platform and AuNPs –polyaniline as a tracer label for amplification in the detection of the same gene[30]. Moreover, a film of ZrO_2 deposited onto Au electrode was used for immobilization of the same 21-mer oligonucleotide specific to *M. tuberculosis* with a detection limit of 0.065 ng/µL of target DNA concentration and of genomic DNA as low as 1 ng/µL[31]. All developed DNA based electrochemical sensors for TB detection until now were based on hybridization of *M. tuberculosis*-specific gene segment with the bio-receptor. Clearly, this indicates that before detection, one has to first isolate *M. tuberculosis* and second extract and amplify a genetic material using molecular techniques, such as PCR (Polymerase Chain Reaction). The sensitivity of the above biosensors could be high; however, the sample preparation procedure requires extra reagents, time, and labour.

Electrochemical immunosensors have been developed based on voltammetry as a detection method, but using different electrode types: screen printed carbon electrode[32] and modified graphene oxide[25]. The detection principle for both electrodes was similar i.e. based on antigen-

antibody specific interaction. *M. tuberculosis* specific proteins were served as antigens. Despite being specific, antibody-based sensors require the production of antibodies in large quantities, which is time-consuming and expensive, and there is a high demand for a high-throughput and low-cost method for generating affinity reagents.

There have only been a few reports on electrochemical detection of MPT64 antigen using different aptamer sequences[33] and various complex surface chemistries[34-36], including electropolymerized poly(3,4-ethylenedioxythiophene) doped carbon nanotubes, gold nanoparticles decorated with fullerene-doped polyaniline, and graphene modified iron-oxide chitosan hybrid nanocomposite film deposited on fluorine tin oxide.

1.3 Objectives and structure of the thesis

The overall goal of the thesis was to develop and evaluate a new method for rapid, specific, and sensitive detection of *M. tuberculosis* secreted protein MPT64 using an impedance aptasensor with specific bio-recognition elements. The specific objectives to reach the goal of this thesis were:

• Select sensitive and specific ssDNA aptamers against MPT64 using the systematic evolution of ligands by exponential enrichment (SELEX) and DOT-BLOT technique. • Perform cloning, sequencing, and bioinformatics analysis of the selected pool of ssDNA aptamers.

• Characterize selected specific ssDNA aptamers using ELONA and Surface Plasmon Resonance (SPR) and validate the affinity of the aptamer using clinical sputum samples. • Optimize the surface chemistry for the aptamer immobilization on the gold-coated interdigitated electrode (IDE) surface using EIS and Biological Field Effect Transistor (Bio FET).

• Study optimization parameters of the aptasensor such as specificity, sensitivity, type of buffer, and detection time and evaluate analytically using spiked serum samples. • Integrate

selected aptamers with the IDE using the optimized surface chemistry and test the aptasensor using clinical TB and non-TB samples with a portable potentiostat. • Study integration of the developed aptasensor with a fluidic chamber.

The PhD thesis comprises six chapters. The first is an introduction that gives an overview of TB diseases, with a comparison of current detection methods and emerging detection techniques.

Chapter 2 gives a detailed review of TB biomarkers, principles of electrochemical biosensors, and EIS as a detection technique. The chapter also discusses aptamers as a bio-recognition element.

Chapter 3 describes the selection of MPT64 aptamers using SELEX, characterization using DOT-BLOT, ELONA, and SPR techniques. The chapter also discusses the application of ssDNA aptamers in the detection of *M. tuberculosis* secreted protein MPT64.

Further, Chapter 4 gives a detailed study on surface chemistry optimization of ssDNA aptamer immobilization on the electrode surface. It also provides a detailed study on specificity and sensitivity studies of the developed electrochemical aptasensor. The chapter presents results on using the developed aptasensor in spiked human serum samples for the detection of MPT64.

Chapter 5 describes the results of the optimization of detection time and topographical studies of the modified electrode with and without target protein. The chapter also presents the validation of the results of the aptasensor on clinical TB and non-TB samples using a portable potentiostat and IDEs.

Chapter 6 provides the preliminary work on the design and fabrication of the fluidic chamber. The chapter investigates the integration of the IDE electrodes with the chamber and gives suggestions on the optimal flow rate of the liquid inside the chamber for the better performance of the aptasensor.

Lastly, Chapter 7 briefly provides a summary of the conclusions of this research, and suggestions for future research.

Type of method
Sub-division of type of method
Type of technique
Recognit ion
molecule
Disadvantage Advantage Reference

Smear
microscopy *
Acid-fast
bacilli smear microscopy
Sputum smear microscopy
Cell
staining
Low sensitivity, not specific to *Mtb*

Sophisticated
Good in poor resource settings[37]

Culture method *

Blood

Automated Bactec MGIT 960 Bacterial growth

Automated Mb/Bact system Bacterial growth

Automated Esp culture system Bacterial growth

automated Bactec 460 Bacterial
Semi
growth
instrument,
contamination,
disposal of radioactive material
Sophisticated
instrument,
contamination,
disposal of radioactive material
Sophisticated
instrument,
contamination,
disposal of radioactive material
Sophisticated
instrument,
contamination,
disposal of radioactive material
Sophisticated
Decrease in numbers of false positive results

Decrease in numbers of false positive results

39

Decrease in numbers of false positive results

40

Decrease in numbers of false positive results

41

sample analysis based
method
Bacterial detection
Bactec Myco/F Lytic Blood Culture
Bacterial growth
instrument,
contamination,
disposal of radioactive material
Decrease in numbers of false positive results

42

28

Type of method
Sub-division of type of method
Mediated
Type of technique
Recognit ion
molecule
Disadvantage Advantage Reference Response to multiple

interferon gamma (IFNg)
detection Mediated interferon gamma (IFNg)
detection

T-SPOT TB test Antibody No discrimination of latent TB from active

QuantiFeron TB Antibody No discrimination of latent TB from active
antigens and discrimination between *Mtb* and environmental mycobacteria [43-45]
Response to multiple antigens and discrimination between *Mtb* and environmental
mycobacteria [46]

Molecular method
Nucleic acid amplification test (PCR, RT-PCR)

DNA
sequencing
Amplification of TB signature genes

Xpert MTB/RIF assay *

Genotype MTBDR plus

DNA hybridization (microarrays)

Whole genome sequencing
DNA
hybridiza tion

DNA
hybridiza tion

DNA
hybridiza tion

DNA
hybridiza tion

DNA
hybridiza tion
Sophisticated
instrument and expensive reagents

Sophisticated
instrument and expensive reagents

Sophisticated
instrument and expensive reagents

Sophisticated
instrument and expensive reagents

Sophisticated
instrument and expensive reagents
Information of size and sequence of a gene and drug resistance can be obtained [47-52]
Information of size and sequence of a gene and drug resistance can be obtained [53]
Information of size and sequence of a gene and drug resistance can be obtained [54]
Information of size and sequence of a gene and drug resistance can be obtained [55]
Information of size and sequence of a gene and drug resistance can be obtained [56 57]

29

Type of method
Sub-division of type of method
Type of technique
Recognit ion
molecule
Disadvantage Advantage Reference

Skin patch
Tuberculin skin test (TST)
Specific gene sequencing

One-Step TB Test Kit; Tell Me Fast *MTB*
DNA
hybridiza tion

Antibody
Sophisticated

	instrument and expensive reagents	
	Follow-up visit required; a wide range of sensitivities and specificities	
	Information of size and sequence of a gene and drug resistance can be obtained	[58]
	No sample preparation/treatment required	[59]
Immune based method	Immunochro matographic IgG/IgM Test Device; Capilia TB; SD Bioline TB AG Mpt64; SD TB IgG/IgM; BD MGIT	
Antibody	No discrimination between MTB species	
	Mutation or deletion of the target gene can result in false negatives	
		[22 60 61]
Electroche mical detection	Differential pulse voltammetry (DPV)	
	DPV	
	DPV	
	Electropolymerised Poly(3,4-ethylenedioxythiophe ne) doped with carbon nanotubes	
	A sandwich scheme based on gold nanoparticles decorated with fullerene-doped polyaniline	
	Graphene modified iron-oxide chitosan hybrid nanocomposite film deposited on fluorine tin oxide	
	aptamer 77 nucleotid es	

aptamer 35
nucleotid es

aptamer 77
nucleotid es
Relatively complex surface chemistry. The sensor needs to be validated in real TB samples.

Relatively complex surface chemistry. The sensor needs to be validated in real TB samples.

Relatively complex surface chemistry. The sensor needs to be validated in real TB samples.
Detection limit within the clinical detection range

34

Detection limit within the clinical detection range

35

Detection limit within the clinical detection range

36

30

Type of method
Sub-division of type of method
Type of technique
Recognit ion
molecule aptamer

Disadvantage Advantage Reference Simple surface chemistry,

EIS
IDM bare gold electrode with MCH as co-adsorbent
40
nucleotid es
The sensitivity still needs to be improved
detection limit within the
clinical detection range, the
sensor was validated in
clinical samples This work
* - routinely used assays in anti-tuberculosis dispensaries approved by WHO. **Table 1. 1**

Overview of TB detection methods described in the literature.

1.4 Role of Collaborators

This thesis is based on my own work and was written by me. Collaborations had an important role in this research. All aspects of this thesis have received advice and have been reviewed by main supervisor Dr. Damira Kanayeva, co-supervisors Dr. Daniele Tosi and Dr. Claude Nogues. Several contributions were also received from the colleagues working at the Laboratory of Biosensors and Bioinstruments at National Laboratory Astana of Nazarbayev University. A full list of my collaborations and publications is listed in section 1.5. I conducted literature review, performed experimental procedures presented in Chapters 3, 4, 5 and 6. The manuscripts associated with this thesis were prepared by myself, with the support provided by co-authors as described below. Suggestions and feedback on manuscripts were provided by my supervisors: Dr. Damira Kanayeva, Dr. Daniele Tosi, Dr. Pedro Estrela and Dr. Claude Nogues; collaborators: Dr. Pawan Jolly, Dr. Ronghui Wang, Prof. Yanbin Li and Prof. Luis Rojas Solorzano. Meiirbek Islamov supported me with the CFD modelling and contributed to the paper published in *Biosensors* journal. Aliya Bekmurzayeva helped me with the selection procedure of the DNA aptamers and contributed to the paper published in *Tuberculosis* journal. Dr. Bakhyt Matkarimov supported me in bioinformatics analysis of aptamer sequences. Dr.

Kanat Dukenbayev helped me with the analysis of the AFM imaging. Dana Akilbekova helped me with the analysis of sputum clinical samples. The regional anti-Tuberculosis Dispensary's (Astana, Kazakhstan) chief doctor Anna Tsepke helped me in providing with the clinical samples and laboratory space in the hospital. The laboratory technicians of the regional anti Tuberculosis Dispensary's (Astana, Kazakhstan) supported me with the AFB staining microscopy results.

1.5 Thesis outputs

Journal articles

[1] Sypabekova, M., Jolly, P., Estrela, P., Kanayeva, D. 2019. Electrochemical aptasensor using optimized surface chemistry for the detection of *Mycobacterium tuberculosis* secreted protein MPT64 in human serum. *Biosensors & Bioelectronics*, 123, 141-151. https://doi.org/10.1016/j.bios.2018.07.053

[2] Sypabekova, M., Korganbayev, S., Blanc, W., Ayupova, T., Bekmurzayeva, A., Shaimerdenova, M., Dukenbayev, K., Molardi, C., and Tosi, D. 2018. Fiber optic refractive index sensors through spectral detection of Rayleigh backscattering in a chemically etched MgO-based nanoparticle-doped fiber. *Optics Letters*, 43, (24), 5945-5948. https://doi.org/10.1364/OL.43.005945

[3] Korganbayev, S., Ayupova, T., Sypabekova, M., Bekmurzayeva, A., Shaimerdenova, M., Dukenbayev, K., Molardi, C., and Tosi, D. 2018. Partially etched chirped fiber Bragg grating

(pECFBG) for joint temperature, thermal profile, and refractive index detection. *Optics Express*, 26, (14), 18708-18720. https://doi.org/10.1364/OE.26.018708

[4] Shaimerdenova, M., Bekmurzayeva, A., Sypabekova, M., Tosi, D. 2017. Interrogation of coarsely sampled tilted fiber Bragg grating (TFBG) sensors with KLT", *Optics Express*, 25 (26), 33487-33496. https://doi.org/10.1364/OE.25.033487

[5] Islamov, M., Sypabekova, M., Kanayeva, D., Rojas-Solórzano, L. 2017. CFD modeling of chamber filling in a micro-biosensor for protein detection. *Biosensors*, 7(4). https://doi.org/10.3390/bios7040045

[6] Sypabekova, M., Bekmurzayeva, A., Wang, R., Li, Y., Nogues, C., & Kanayeva, D. 2017. Selection, characterization, and application of DNA aptamers for detection of *Mycobacterium tuberculosis* secreted protein MPT64. *Tuberculosis*, 104, 70-78. https://doi.org/10.1016/j.tube.2017.03.004

Patent

[1] Kanayeva D, Sypabekova, M, Bekmurzayeva, A, Li, Y. 2019. Aptamers for determining bacterial cell *Mycobacterium tuberculosis* based on secreted protein MPT64, composition containing DNA aptamer and method of detecting mycobacteria in a clinical sample. IPC No. C12P 19/34 (2006.01), C12Q 1/00 (2006.01), Ministry of Justice of the Republic of Kazakhstan, Patent No. 33639, Oct 30, 2017.

Conference presentations

[1] Sypabekova, M., Kanayeva, D. 2018. Portable EIS aptasensor for the detection of immunogenic protein MPT64 from *Mycobacterium tuberculosis*. 28th Anniversary World Congress on Biosensors. Miami, FL, USA.

[2] Sypabekova, M., Bekmurzayeva, A., Kanayeva, D. 2016. Impedance based biosensor for the detection of immunogenic protein MPT64. 26th Anniversary World Congress on

Biosensors. Gothenburg, Sweden.

Chapter 2. Literature review

This Chapter presents an overview of TB biomarkers. It also introduces a brief introduction on electrochemical biosensors, EIS and aptamers as a biorecognition element, which has been used as the foundation for the aptasensor mentioned in this thesis.

Part of the work presented in this Chapter was published in[2].

2.1 TB candidate biomarkers

A biomarker is a biological characteristic that can be quantified and evaluated as an indicator of normal biological processes, pathogenic processes, or pharmacologic responses to a therapeutic intervention[62]. Biomarkers have been used as diagnostic tools to predict clinical outcomes of the disease state and treatment.

Currently, such biomarkers for TB diagnosis include 23 kDa MPT64, 6 kDa early secreted antigenic target (ESAT-6), 10 kDa culture filtrate protein (CFP-10), and antigen-85 complex. They are predominantly secreted immunogenic proteins of *M. tuberculosis* and being investigated for potential application in skin patch test, immunochromatographic assays, immunohistochemical analysis, PCR, and ELISA[63].

2.1.1 MPT64

MPT64 is one of the secreted immunogenic protein of *M.tuberculosis*[7 64, 1] with a molecular weight being reported differently in the literature: 22.3 kDa[65]; 23 kDa[66], 23.497 kDa[67], 24 kDa[68], and 28 kDa[69]. The protein is highly specific for *M. tuberculosis* Complex (MTBC) species and it is not found in NTM[66 70 71]. MTBC species comprise *M. tuberculosis*, virulent *M. bovis*, *M. africanum*, some substrains of *M. bovis* bacilli Calmette-Guérin (BCG). MPT64 is expressed and secreted by the actively dividing *M. tuberculosis* along with other 33 predominantly secreted proteins[66 68 72]. Such secreted proteins, also called antigens, are recognized by the immune cells and initiate the first host immune response. For instance, the production of mycobacterial antigens can stimulate the proliferation of T-cells and the release of interferon

gamma (IFN-g) from peripheral blood mononuclear cells (PBMC)[70]. Studies are being carried out on the investigation of MPT64 as a potential candidate vaccine for TB[73-76]. The whole genome comparison studies showed that some regions of the genome that are present in MTBC

could be absent in BCG substrains and several NTM[77]. These gene segments are called regions of differences (RD) and the product of that gene in the form of proteins are called RD proteins. MPT64 is an RD protein which is absent in some BCG strains[78-81]. MPT64 protein is secreted by *M. tuberculosis* at an early stage and was shown to account for about 8% of the total protein found in the supernatant culture filtrate[82]. Using bioinformatics tools it was found that there were no similar MPT64 epitopes in MTBC suggesting that the protein might be unique[82]. The protein is essential for mycobacterial its survival and persistence in the host cell. *M. tuberculosis* has an ability to inhibit the apoptosis of infected macrophages by deactivating the expression of apoptotic cytokines therefore promoting the survival and virulence of *Mycobacteria*[83]. Studies showed that exosomes released from infected macrophages contain

mycobacterial proteins, including MPT64. It has been predicted that the existence of MPT64 and other TB proteins could be associated with the function of these proteins during the establishment and maintenance of intracellular infection[84]. It has been also reported that these TB-protein enriched exosomes were found to be released into the serum, which opens up the window for diagnostics based on biomarker identification in serum exosomes to reveal active TB in patients[83]. According to the latest multiple reaction monitoring assays, the clinical diagnostic level of MPT64 protein in isolated exosomes from the serum was at a sub-nanomolar (nM) range[85].

Taking into consideration its biological characteristics, MPT64 has been studied and used in the diagnosis of TB. The specificity, sensitivity, detection time, availability, and price of such diagnostic methods based on the identification of the MPT64 protein vary. Current TB diagnosis based on the detection of MPT64 has been used in immunochromatographic, immunohistochemical, and ELISA[63 86-88]. These methods are based on antigen/antibody interactions. Although routinely used, antibodies have certain limitations in their use in diagnostic tests in low resource settings: they are expensive to produce, temperature sensitive, can easily undergo functional modifications, have reduced shelf life (less than 6 months), and often there is batch to batch variations. Other detection studies based on reverse transcription polymerase chain reaction (RT-PCR) targeting the MPT64 gene offer great sensitivity and specificity[87 89]. However, they are cumbersome in resource-limited settings and require a relatively expensive set of reagents and trained personnel.

2.1.2 CFP-10 and ESAT-6 complex

Culture filtrate protein CFP-10 (10kDa) and early secreted antigen ESAT-6 (6kDa) are two small proteins involved in *M. tuberculosis* virulence. They are one of the most abundant antigens of *M. tuberculosis* grown in the culture[1]. These proteins are present in *M. kansasii, M. szulgai, M. marinum,* and *M. riyadhense* but absent in *M. bovis* BCG and most MOTT[90 91]. CFP-10 and ESAT-6 are encoded by genes aligned in pairs in the *M. tuberculosis* genome. The product of the genes is then secreted by specialized transport system[92 93]. ESAT-6 is a globular protein, whereas CFP-10 is less structured and they form one to one complex[86]. One of the

main characteristics of this complex is that the C-terminus of CFP-10 forms a long flexible arm, which plays an important role in a cell surface attachment specifically binding to macrophages and monocytes[92]. These proteins like MPT64 also stimulate the production of T-cells and are among the candidate of vaccines for TB[94].

2.1.3 Ag85 complex

M. tuberculosis Antigen 85 (Ag85) complex involved in biological processes such as in cell wall biosynthesis and immunogenic responses[95]. The complex comprises three variations of Ag85 proteins: A, B, and C. They are secreted and can be found in a phagosomal space and on a bacterium's cell wall[96 97]. The immunogenic response of the host is altered when Ag85 complex binds to plasma fibronectin, an extracellular matrix glycoprotein, or immunoglobulin G. This interaction appears to reduce phagocytosis of *M. tuberculosis* thereby promoting infection[98 99]. The Ag85 expression is essential for the intracellular survival of *M. tuberculosis* within a macrophage[100] and possesses mycolyltransferase activity. It also catalyzes the synthesis of the most abundant glycolipid of the mycobacterial cell wall, trehalose 6,6-dimycolate which is located at the external layer of the cell wall[101]. The binding sites of fibronectin and trehalose are located on different domains of antigen 85B. Although antigen 85B is found primarily in the cell wall of *M. tuberculosis*, it also circulates in the blood, where it complexes with plasma fibronectin[98]. The composition of the active site of all three variants, Ag 85A, B, and C, is highly conserved[96]. Ag85B is a 30 kDa protein composed of 285 residues. Structurally, it forms an α-β hydrolase fold with a core of 8 β sheets surrounded by α helices and a catalytic triad of Ser-126, His-262, and Glu-230[102]. Three variants of Ag85 are encoded from separate genes, and are expressed in different concentrations, generally in a 3:2:1 ratio of B:A:C. However, this ratio varies in response to changes in the environment. Even though B

is highly expressed, C is 8 times more biologically active than B. The important fact is that all three variants in combination are necessary for evading immune response within a host[97].

2.2 Electrochemical biosensor

Quantification of biological or biochemical processes is extremely important for diagnostic applications. For this purpose, the biological information needs to be converted to an easily

processed electronic signal [103]. This type of conversion of biological response into a quantifiable and processable signal is performed by an analytical device-biosensor[104]. Biosensors are now being widely used in biomedical diagnosis, the point of care monitoring (PoC) of disease progression and treatment, drug discovery, environmental monitoring, food control, forensics, and biomedical research[105]. The combination of a biosensor with high-affinity bioreceptors

enables a sensitive and selective detection of a range of analytes. A typical biosensor consists of a bioreceptor (cell, nucleic acid, antibody, enzyme) that specifically binds to an analyte (antigen, protein, ion, nucleic acid), interface (electrodes, nanowire array, nanoparticles, and FET devices), where a specific biological event takes place and the transducer that converts biological signal into an electronic one. The electronic signal is then amplified by a detector and sent for processing[103 106] (**Figure 2.1**). The biosensor can be used to detect an analyte in a large

variety of samples including cell culture, human samples (blood, saliva, urine), food and environmental samples. Based on the detection mechanism (mechanical, magnetic, optical, or electrochemical) various types of biosensors were developed over the last decade.

The first research line on biosensors started with the introduction of the electrochemical glucose sensor, the only realized cheap handheld PoC device[107] that is widely used with added improvements since the 1960s[108]. The main advantage of realizing other PoC sensing devices is the miniaturization of the setup and expensive cost of production to be used by patients/doctors in house/on field bypassing the use of expensive equipment in laboratories. Electrochemical biosensors in addition to the above advantages have cheap production of microelectronic circuits, easy interface with normal electronic read-out, and processing[103]. The recent developments in electrochemical biosensors allowed creating sensors with smaller dimensions which increased the signal to noise ratio offering new generation highly specific and reliable sensors and sensor arrays[109]. These biosensors offer an attractive way to analyze the biomolecule concentration as the interacting analyte of interest produces an electrical signal proportional to the analyte concentration.

Electrochemical measurement in such biosensors is based on studying transportation of charges across the electrode and electrolyte interface resulting in a change of the electrical and chemical properties[110]. A typical electrochemical sensor consists of a sensing electrode

(working electrode: *WE*), reference electrode (*RE*) connected to a high-input-impedance potentiostat, and a counter electrode (*CE*), which is used to complete the circuit for current flow[111]. *WE* is the electrode where the biochemical reaction takes place. The potential is set between *WE* and *RE*. The current is passed and measured between the *CE* and the *WE*. The *CE* helps to maintain a stable voltage between the *WE* and the *RE*. Such configuration allows the measurement of the potential of the *WE* against a known *RE* without compromising *RE* stability by passing a current through it (**Figure 2.2**). *RE*, *CE*, and modified *WE* are usually immersed in an electrolyte with/without redox markers and each of them connected to a potentiostat. Redox markers are special indicators that can exchange electrons with the *WE* and, thereby, contribute to the detection of the current. This happens when the redox markers come close to the *WE* surface from the bulk electrolyte and initiate the electron transfer. The electron transfer on its turn results in the detection of current.

A range of electrochemical techniques can be used for biosensing applications, namely amperometric (measurable current), potentiometric (measurable potential or charge accumulation), conductometric (measurable conductive properties of a medium between electrodes), impedimetric (measurable impedance resistance and reactance), and field-effect (uses transistor technology to measure current at a gate electrode)[2 106 112 113]. The impedimetric technique was used within the scope of this thesis since it can provide low cost, low power, scalable, and highly sensitive (without requiring pre-labelling of the analytes) measurement with minimal hardware demand[114].

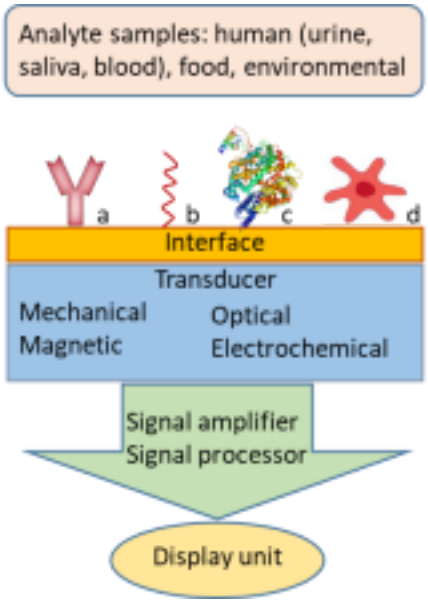

Figure 2.1 A schematic overview of biosensor components. Analyte samples with specific biomolecules interact with a bioreceptor (a: antibody; b: nucleic acid; c: enzyme; d: cell) immobilized on the interface and create a biological signal. The biological signal is converted into an electronic signal via a transducer. The electronic signal is then amplified and processed into a readable signal and displayed.

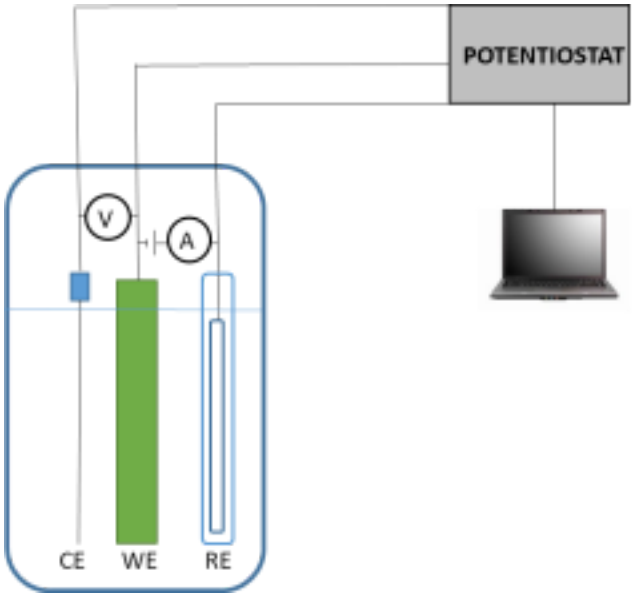

Figure 2.2 Electrochemical set up for a three-electrode system.

2.2.1 EIS as a detection technique

EIS is the technique used in impedimetric electrochemical biosensors. EIS has numerous advantages over other detection techniques. It is a label-free technique and the signal in EIS

can

be recorded within a small change of analyte binding event based not only on molecular interaction level but also on electron/charge transfer levels. The latest studies on EIS based biosensors exploit improved binding strategies, optimized surface chemistry for the accurate and sensitive sensing down to attomolar range[115-118]. The EIS based biosensors have been used in studies for the detection of different cancer biomarkers, bacteria, toxins, and polluting agents[119].

Impedance is a frequency dependent resistance to current flow between the electrodes and the electrolyte. In EIS, impedance is obtained by applying a voltage over a wide range of AC potential frequencies (typically from 1 Hz to 100 MHz) and measuring the resulting current (**Figure 2.3**). For the biosensor development, it is possible to select a single frequency at which the device collects the best possible response from the biological reaction[120]. The frequency response provides information on a biochemical interaction between the analyte and the bioreceptor and creates charge transfer processes from the solution to the electrode surface, solution resistance, as well as diffusion transport of species to and from the bulk solution and double layer capacitance formation[121].

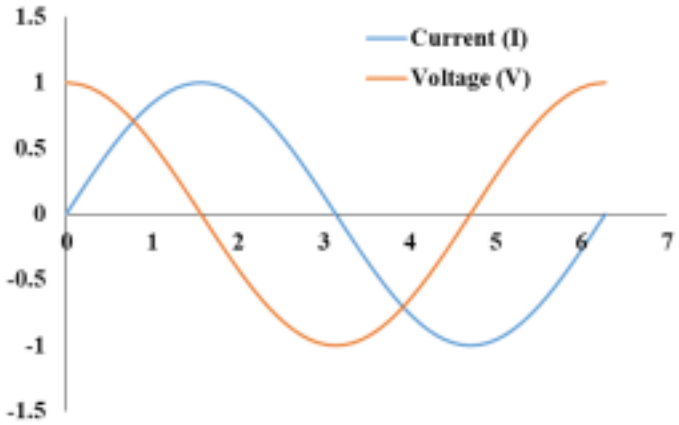

Figure 2.3 A typical graph of an AC signal of the applied voltage and obtained current response during the impedance measurement.

The AC excitation voltage signal can be expressed as a function of time *(V(t)* and has the formula*:*

$$V(t) = V_0 \sin(\omega t) \quad (1)$$

V is the potential at time *t*, V_0 is the amplitude of the signal, ω is the angular frequency expressed in radians/seconds and has the relationship with frequency (*f*) expressed in Hertz (Hz) ($\omega = 2\pi f$). The resulting AC current signal *(I (t))* is shifted in phase (φ), with different magnitude (I_0) and can be expressed as follow:

$$I(t) = I_0 \sin(\omega t + \varphi) \quad (2)$$

Following Ohm's law, the impedance of the system can be calculated as follow:

$$Z = \frac{V(t)}{I(t)} = \frac{V_0 \sin(\omega t)}{I_0 \sin(\omega t + \varphi)}$$

$$I_0 \sin(\omega t + \varphi) = V_0 \sin(\omega t) \quad (3)$$

The impedance of the system is, therefore, expressed in terms of the magnitude (Z_0) and the phase shift (φ). Using the Euler's relationship, where *j* is an imaginary number

$$\exp(j\varphi) = = \cos\varphi + j\sin\varphi \quad (4)$$

the impedance (*Z*) can be expressed as a complex function

$$Z = \frac{V(t)}{I(t)} = \frac{V_0 \sin(\omega t)}{I_0 \sin(\omega t + \varphi)}$$

$$I_0 \sin(\omega t + \varphi) = I_0 \exp(Z\varphi) = I_0 (\cos\varphi + j\sin\varphi) = Z' + ZZ'' \quad (5)$$

which is the sum of real and imaginary parts. Therefore, the system can analyze both real and imaginary parts of the impedance, which corresponds to the electrical resistance and reactance respectively[111].

Impedance measurements mostly can be performed in two ways: Faradaic and Capacitive (non Faradaic)[114]. The former approach includes the amplification of the change by the addition of a

redox probe, whereas the latter approach does not require the addition of the redox probe into the analytical solution[114]. The Faradaic mode based on measuring changes in charge transfer resistance (R_{ct}) which is generated by the interaction between the analyte and the bio-receptor on the electrode surface. Faradaic mode involves the transportation of redox species between the electrode and electrolyte solution (**Figure 2.4**). This happens as a result of the application of voltage and modulation of the potential of the *WE*. The potential of the *WE* can create

reduction current or an oxidation current depending on where the potential pushed i.e. towards the more negative or positive values, respectively.

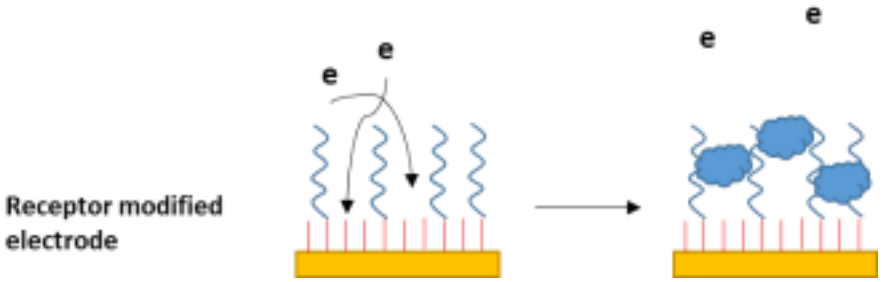

Figure 2.4 A schematic representation of an electron transfer promotion and inhibition in Faradaic mode on a receptor modified electrode with (right) and without (left) target analyte.

The non-Faradaic mode monitors only capacitive changes. In such configuration, the importance is given to double layer capacitance rather than to R_{ct}[122]. It involves the application of a potential to the electrode, which causes the redistribution of the charges on the electrolyte in close proximity to the electrode surface, which in its turn leads to changes in surface potential and creation of an electrical double layer capacitance (**Figure 2.5**).

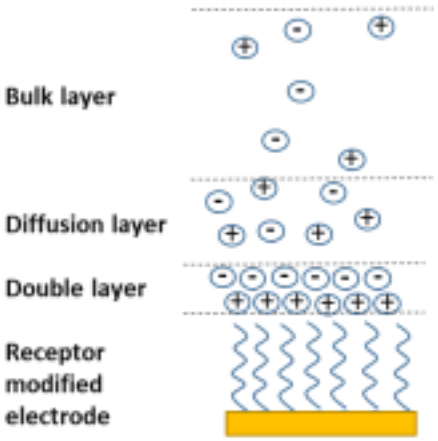

Figure 2.5 Schematic overview of an electrical double layer of a receptor modified electrode electrolyte interface.

Results obtained from EIS can be plotted (Nyquist plot), fitted, and modelled with an electrical equivalent circuit, in most cases Randles circuit (**Figure 2.6**), where R_s is the solution resistance which is not affected by the binding process and depend only on the solution along the distance between the *WE* and *RE*, R_{ct} is the resistance for electron transfer, Z_w is the Warburg impedance

gives information about the diffusion of a redox couple through the surface layer, and C_{DL} is the double layer capacitance which depends on the thickness of the modified layer.

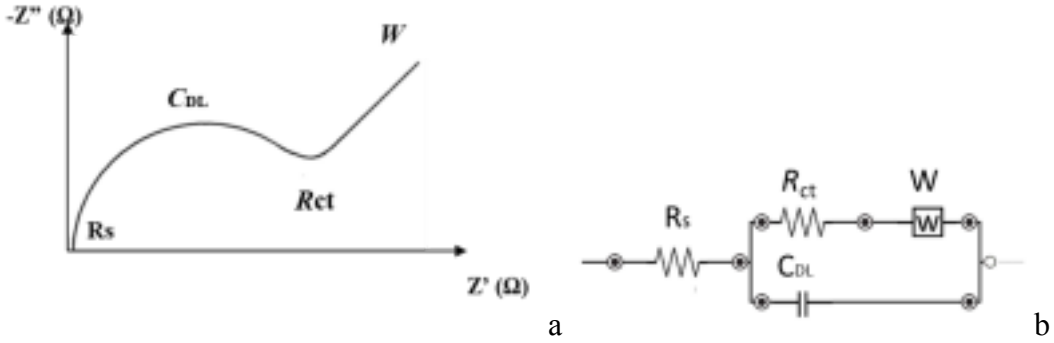

Figure 2.6 (a) A typical Nyquist plot with a semicircle region followed by a straight line. The semicircle part indicates a charge-transfer limited process in the high-frequency range and the linear part indicates a mass-transfer limited process in the low-frequency range. The R_s (solution resistance) and R_{ct} (charge transfer resistance) values could be determined from the Nyquist plot. The R_s is not affected by the binding process and R_{ct} is an electrical parameter in analyzing the impedance signal change for the detection of protein; (b) Randles equivalent circuit, where R_s is solution resistance, R_{ct} is charge transfer resistance, Z_w Warburg impedance, and C_{DL} the double layer capacitance.

2.2.2 Aptamer as a bio-recognition element

Aptamers are single-stranded oligonucleotides (either DNA and RNA) that have abilities to specifically bind to a broad range of targets[123-125] with a high affinity[126]. Aptamers are synthesized *in vitro* using a SELEX procedure[123]. This method includes three main stages: (i) incubation of a random library with the target; (ii) separation of bound aptamers from unbound ones; (iii) amplification of bound sequences using PCR [126] (**Figure 3.1**). Aptamers have qualities that can overcome some disadvantages of antibodies. For example, aptamers are synthesized *in vitro* from a library that contains large numbers of random sequences. This

alleviates the use of animals during the selection process compared to antibodies, and their properties can be changed on demand: aptamers that can bind their targets in non-physiological conditions can be selected. It is possible to select aptamers against targets that are non-immunogenic or toxic to animals. Production of selected aptamers is done by chemical synthesis, and, thus, they have less batch to-batch variation and are purer. Furthermore, they can be massively synthesized once selected,

and this is more cost-effective than the production of antibodies. Aptamers made from nucleic

acids are more stable than antibodies, and they can be stored in ambient temperatures. In addition, they are smaller in size, and their affinities are not affected by labelling[127-129]. Because of these properties, aptamers are used in areas that include functional studies of proteins, therapeutics, diagnostics, and biosensing[124 126]. Aptamers can find application in biosensing areas mainly because they can be selected and used under any pre-defined conditions, and they can be easily immobilized to obtain a custom-made surface. Moreover, they can be reused since they are capable of refolding to the native conformation after one round under certain denaturing conditions[128]. To date, aptamers have been synthesized against targets that include metal ions, small organic molecules, proteins, peptides, nucleic acids, polysaccharides, virus particles, whole cells, and even tissues[126 130].

2.2.3 Immobilization of aptamers on a transducer surface

The immobilization of aptamers on the transducer surface plays a key role in aptasensor development. Surface chemistry has been an important aspect in the development of a successful aptasensor. The accurate and proper control of each immobilization step is important for obtaining a good sensitivity, selectivity, and stability of the aptasensor. Many electrode surfaces have been used as a transducer platform for aptamer immobilization including gold, gold nanoparticles, glass, graphene, carbon nanotubes coated electrodes. The most common aptamer immobilization techniques are physical adsorption, covalent bonding with the use of self-assembled monolayers (SAM), and interaction based on complex formation between avidin-biotin, surface activation with EDC/NHS, and entrapment of aptamer within the polymer[131].

The work in this thesis uses a gold-coated electrode surface for the aptasensor development and covalent immobilization of aptamers using SAMs. SAMs on gold surfaces form a highly stable

and well-ordered complex. The thickness of the layer could be controlled and optimized for better sensitivity and specificity. The interaction between SAM and the gold surface is based on the strong bond between the sulphur and gold atoms. The well-organized layer of SAM on the gold surface is usually formed in no less than 12-16 h[132] [133] with a tilt angle between the hydrocarbon chains and the electrode surface being at 30°[134]. The other end of the SAM, not tethered to the gold surface, could be linked to functional groups, which allows the aptasensor to have a controlled surface distribution and thickness. The co-immobilization of SAMs and the DNA probe have led to the establishment of mixed SAMs[135]. The composition of mixed SAMs

and their careful tuning allows monitoring a number of functional groups available for binding. The choice of spacer molecules between the DNA probe and the gold surface can influence the surface property by increasing the chemical reactivity and decreasing the non-specific binding[135].

2.2.4 Interdigitated electrodes as a transducer platform

Interdigitated electrodes (IDEs) are electrodes that consist of two individually addressable interdigitated comb-like electrode structures **(Figure 2.7**) that act as a platform of the transducer of a biosensor device. It is usually made of a metal layer deposited on a substrate (glass, plastic). For biosensor applications, the metal layer is functionalized with special bio-receptors. Since the distance between the anodic and cathodic electrodes are smaller on IDEs, the oxidation and reduction cycle speed is increased, which enables the data collection with high efficiency[136]. Furthermore, the use of IDEs offers a range of advantage over a planar gold surface such as reduced response time and increased impedance change, and enhanced sensitivity[137]. The electrode geometry and spaces between the IDE fingers play an important role in impedance or capacitance measurement. The reduction of inter-electrode (finger) spacing increases the effective electrode area, thereby increasing the sensitivity of the device[138]. Depending on the operating modality, the IDEs can be operated in both Faradaic and non-Faradaic mode. To date, different types of EIS biosensors employing IDEs have been reported including biosensors for bacterial cells[139] and viruses[140], immunosensors[141] and aptamer-based sensors[142].

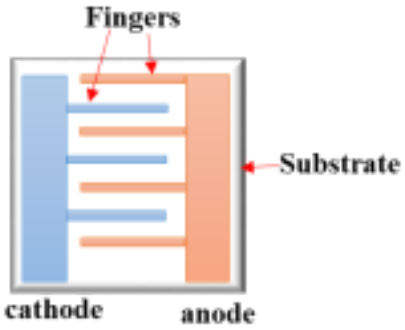

Figure 2.7 Schematic structure of the IDE. Two individually addressable interdigitated comb like electrode structures made of metal deposited on a substrate.

Chapter 3. Selection, characterization, and application of DNA aptamers for the detection of MPT64

This Chapter provides a presentation on the selection of ssDNA aptamers for the detection of MPT64 based on the SELEX methodology. The study also focuses on Dot-Blot, ELONA, and SPR as characterization techniques. The Chapter also describes the validation of the selected aptamers on clinical sputum samples.

The work presented in this Chapter was published in[143].

3.1 Abstract

For the global control of TB, it is important to detect *M. tuberculosis*, an etiological agent of TB. Because of their inherent characteristics, aptamers have emerged as a potential rival for antibodies in therapeutics, diagnostics and biosensing. The present Chapter aimed at selecting and characterizing single-stranded DNA aptamers against MPT64, one of the predominant secreted proteins of *M. tuberculosis*. Aptamers specific to MPT64 were selected *in vitro* using the SELEX method. A selection process was started with a pool of ssDNA library with the randomized 40-nucleotide region. A total of ten cycles were performed and seventeen aptamers with unique sequences were identified by sequencing. Dot Blot analysis was performed to monitor the SELEX process and to conduct preliminary tests on the affinity and specificity of

aptamers. Enzyme-linked oligonucleotide assay (ELONA) showed that most of the aptamers were specific to the MPT64 protein with a linear correlation of $R^2 = 0.94$ for the most selective one. Using SPR, dissociation equilibrium constant K_D of 8.92 nM was obtained. Bioinformatics analysis of the most specific aptamers revealed the existence of a conserved as well as distinct sequences and possible binding site on MPT64. The specificity was determined by testing non target ESAT-6 and CFP-10. Negligible cross-reactivity confirmed the high specificity of the selected aptamer. The selected aptamer was further tested on clinical sputum samples using ELONA and had sensitivity and specificity of 91.3% and 90%, respectively.

3.2 Materials and methods

Figure 3.1 illustrates principles and concepts of selection and characterization of MPT64 aptamers, and four major steps of the experiments: (i) *in vitro* selection of aptamer candidates against MPT64 using SELEX method; (ii) dot blot analysis of affinity of the pool of aptamers from selected SELEX rounds and aptamers with known sequences; (iv) ELONA assay and (iii)

cloning, sequencing, and bioinformatics analysis of aptamers. The methods are described in the following sections.

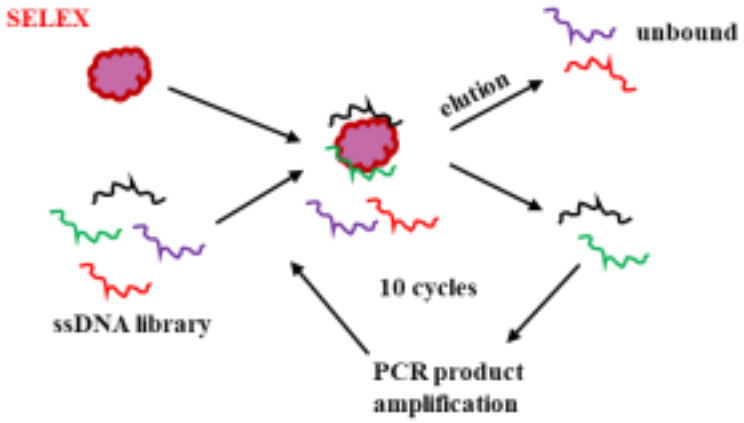

i

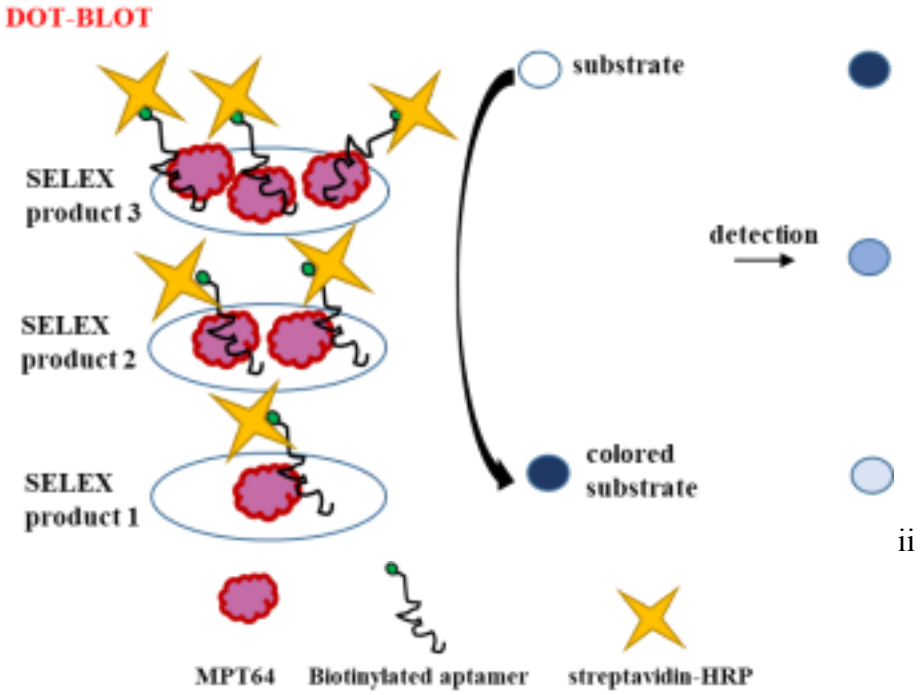

ii

Figure 3.1 A schematic representation of principles and concepts of selection and characterization of MPT64 aptamers using SELEX (i), dot blot (ii), cloning, sequencing (iii), and ELONA techniques (iv).

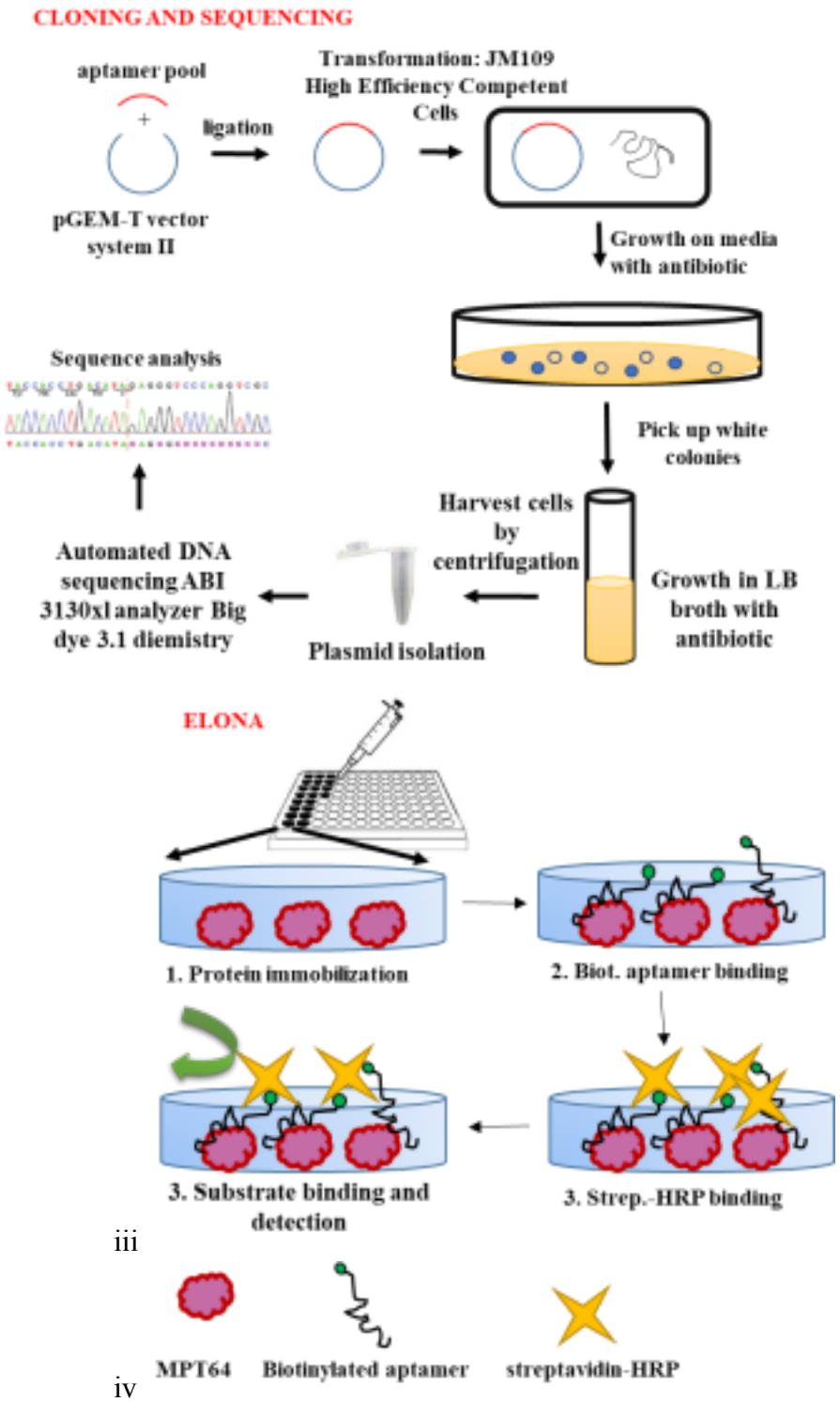

Figure 3.1 (continued) A schematic representation of principles and concepts of selection and characterization of MPT64 aptamers using SELEX (i), dot blot (ii), cloning, sequencing (iii), and ELONA techniques (iv).

3.2.1 Proteins

Target immunogenic protein MPT64 (46kDa) (Rv1980c) (Gene ID: 581375; Accession#: CAA53143) of *M. tuberculosis* H37Rv strain with a concentration of 1 mg/ml was obtained from EnoGene Biotech Co Ltd (Nanjing, China). His and Trx tagged MPT64 protein was purified from recombinant *Escherichia coli* strain by affinity chromatography with >90% purity. According to manufacture, the protein is suitable for use in multiple immunoassay formats, including ELISA, Western Blot, and rapid tests. Non-target ESAT-6 (p463-1) and CFP-10 (p460-1) proteins were purchased from Sunny lab (USA).

3.2.2 DNA library, primers

The oligonucleotide template was synthesized as a single-stranded 80-mer with the following sequence: 5'- TCA CTT CAA ATG TGC GCT TC – N40 – CGT CAA AAC AGG GGG TAG AA - 3', where the central 40 nucleotides represent random oligonucleotides based on equal incorporation of A, T, G, and C at each position. The dsDNAs were obtained by PCR amplification using Forward 5'- TCA CTT CAA ATG TGC GCT TC-3' and Reverse 5'- TTC TAC CCC CTG TTT TGA CG -3' primers. Biotinylated forward primer for Dot-blot analysis and phosphorylated reverse primers to obtain ssDNAs by lambda exonuclease digestion were of the same sequences as forward and reverse primers. Both the library and primers were synthesized and PAGE purified by Integrated DNA Technologies (Coralville, IA, USA).

3.2.3 *In vitro* selection of aptamers

Aptamer candidates against MPT64 were selected using the SELEX protocol based on[144] with slight modifications. SELEX is an oligonucleotide-based combinatorial library approach which has been extensively used to isolate aptamers against various targets including proteins, ions, cells and surface epitopes[145] [146]. This method includes three main stages: incubation of a random library with the target; separation of bound aptamers from unbound ones; and amplification of bound sequences using PCR[147] (**Figure 3.1**).

The DNA was passed three times prior to the selection cycle through a pre-wetted nitrocellulose acetate membrane (0.45 μm HAWP filter, Millipore, MA, USA) in a filter holder ("pop-top", diameter 13 mm, Millipore) in order to exclude filter-binding ssDNA sequences from the library. To initiate *in vitro* selection, ssDNA library was denatured at 95 ^{o}C for 10 min in a thermocycler (Mastercycler gradient, Eppendorf) and was allowed to be cooled

down

approximately to 34 - 38 ^{o}C inside the thermocycler. Denatured DNAs were then incubated with the target protein at 15 rpm on a variable speed rotor (Grant Bio PTR-30, Keison) for 1 h and 45 min at room temperature (for the first cycle). This reaction mixture was then filtered over a HAWP filter and washed with binding buffer (50 mM Tris-HCl; 25 mM NaCl; 5 mM $MgCl_2$; 10 mM DTT; pH 7.5). ssDNA that was retained with the protein on a filter were eluted with elution buffer (0.4 M sodium acetate, 5 mM EDTA, and 7 M urea, pH 5.5) at 70-80 ^{o}C for 5 min twice. Afterwards, the eluted DNA was diluted with an equal volume of dH_2O and was precipitated with ethanol and ammonium acetate and incubated for 1 h at -80 ^{o}C. After centrifugation at 13,000 rpm at 4 ^{o}C for 1 h, the supernatant was discarded, and the pellet was washed twice with 75% ethanol solution and resuspended in dH_2O for further PCR. Amplification conditions were as follow: initial denaturation at 95 ^{o}C for 5 min and a final extension at 72 ^{o}C for 10 min; and 30 cycles of denaturation at 95 ^{o}C for 30 s; annealing at 58 ^{o}C for 45 s and extension at 72 ^{o}C for 45 s. Amplified products were analyzed on non-denaturing 6% Tris-borate EDTA (TBE)-polyacrylamide gels (Invitrogen, CA, USA) at 200 V for 20 min after binding with SYBR Green 1 (Invitrogen, CA, USA). ssDNA was obtained by digestion of PCR products amplified with phosphorylated reverse primers with 5 units of lambda exonuclease (New England Biolabs, Ipswich, MA, USA) per 50 µl reaction. The reaction was done for 1 h at 37^{o}C and then heat inactivated for 10 min at 72 ^{o}C. Digested products were precipitated as above (resuspension of the pellet in binding buffer) and used for the next round of SELEX. 10 iterations of SELEX were performed. For additional rounds of selection, the amount of protein was reduced twice in each cycle: from 4.35 µg to 0.07 µg in a binding buffer (total volume of 150 µl). Incubation time was in the range from 1 h 45 min for the first cycle and 40 min for the last. Incubation conditions, as well as concentrations of the target protein and ssDNA, are listed in **Table 3.1**. The concentration of ssDNA was measured using NanoDrop 1000 Spectrophotometer (ThermoScientific, DE, USA). All procedures (where applicable) were performed in a biosafety level 2 cabinet (Purifier Delta Series Class II, Type A2 Biological Safety Cabinet, Labconco Corporation, MO, USA).

SELEX cycle	Target MPT64 (μg)	ssDNA pool (μg)	Incubation time (min)
1	4.35	35	105
2	2.17	~30	90
3	1.08	~30	60
4	0.54	~30	60
5	0.27	2.9	60
6	0.13	7.1	50
7	0.07	~7	40
8	0.04	10	40
9	0.03	10	40
10	0.03	10	40

Table 3.1 Concentrations of ssDNA and target MPT64 used in *in vitro* selection of aptamers.

3.2.4 Dot blot analysis

Dot blot is a technique that enables identification and analysis of proteins of interest where sample proteins are spotted onto the membrane and hybridized with a probe[148]. The successful interaction results in coloured spots (**Figure 3.1**). Dot blot in this study was used for rapid analysis of an affinity of the pool of aptamers from selected SELEX rounds and aptamers with known sequences. Selected SELEX DNA products were amplified using forward biotin-labelled primers and phosphorylated reverse primers with further digestion using lambda exonuclease to obtain biotinylated ssDNA.

MPT64 protein was applied onto a nitrocellulose membrane (BA85 Protran, 0.45 μm, Whatman, USA) in different concentrations (87, 8.7, and 0.87 μg/ml) for dot blot analysis of SELEX products. For dot blot analysis with known aptamer sequences, 500, 250, 100, 50, 25, 10, 5, and 1 μg/ml of MPT64 protein was applied onto the nitrocellulose membrane. After

immobilization on the membrane, blocking buffer (casein 12.5 g; NaCl 4.5 g; Tris 605 mg; Thimerosal 100 mg) was applied for 45-60 min, and 475 µl of 817 ng biotinylated aptamers from selected cycles were left to incubate for 30 min. After washing three times with 1× KPL (KPL, Gaithersburg, Maryland) washing solution (0.002 M imidazole, 0.02% Tween 20, 0.5 mM EDTA, 160 mM NaCl) the membrane reacted with streptavidin-alkaline phosphatase diluted to 1:500 for 30 min. The membrane was then coated in BCIP/NBT (5-Bromo-4-chloro-3-indoxyl-phosphate and nitroblue tetrazolium) (KPL, MD, USA) substrate for 15 min in the dark after washing. The

results were determined by observation of violet stained spots on the membrane (**Figure 3.2 b, c**). *E. coli* antibodies labelled with biotin served as a positive control (diluted at 1:500) (Meridian Life Sciences, ME, USA), and deionized water served as a negative control.

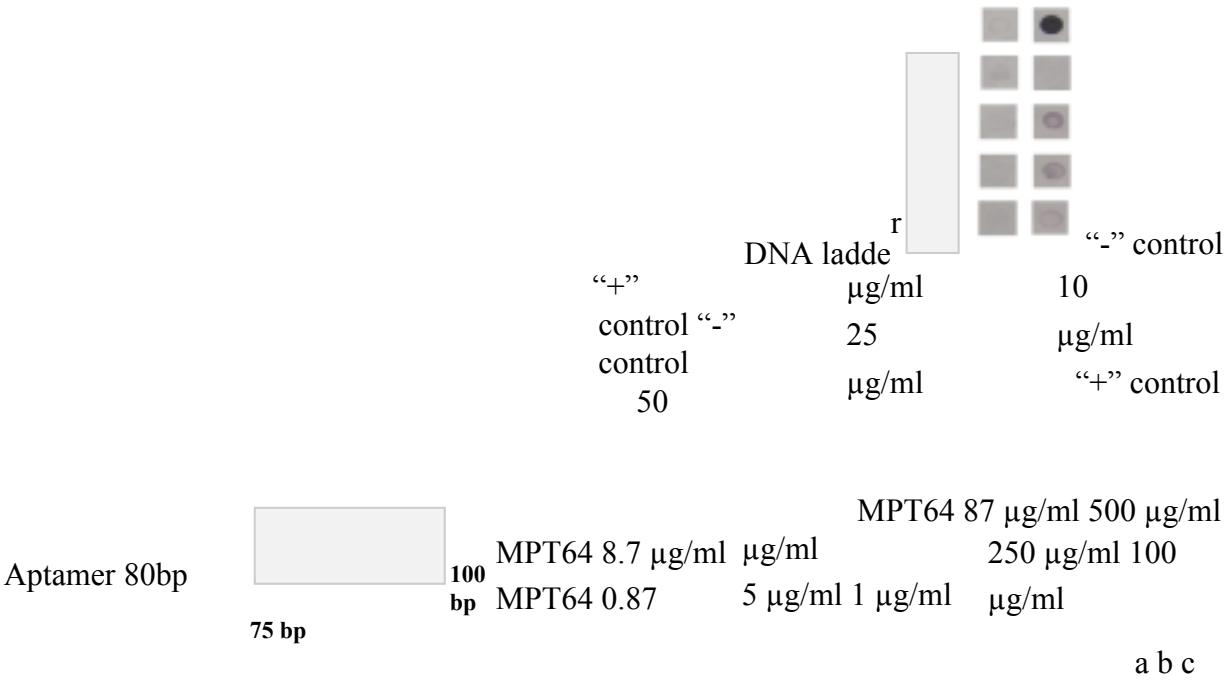

Figure 3.2 (a) 6% TBE-PAGE analysis of PCR products from cycle 6 of in vitro selection of aptamers against target MPT64 by SELEX method stained with SYBR Green I: Lane 1. PCR product of SELEX cycle 6, Lane 2. 25 bp DNA ladder; (b) Dot blot analysis of affinity binding between aptamer pools from the SELEX cycle 5 and target MPT64, and two controls; (c) Affinity evaluation of the ssDNA aptamer sequence (4) using dot blot analysis method. "+" control E. coli antibodies labelled with biotin (diluted at 1:500), "-" control - deionized water.

3.2.5 Cloning

The aptamer pools from SELEX rounds were purified on either 6% TBE gel (Invitrogen) or using Qiaquick PCR Purification Kit (Qiagen, Germany), ligated to pGEM®-T Vector System II and transformed into JM109 High Efficiency Competent Cells according to the manufacturer's manual (Promega, USA) and then incubated at 37 °C overnight. White colonies were picked and streaked on a plate. Individual colonies of the transformed cells were propagated in 5 ml of LB broth with ampicillin (50 μg/ml) for 15 h at 37 °C. The cells were harvested by centrifugation at 8,000 rpm for 5 min, and plasmid DNA was extracted using the QIAprepMiniprep kit (Qiagen, Germany). Ampicillin and IPTG used in cloning were purchased from Calbiochem (San Diego, CA, USA); X-Gal (5-bromo-4-chloro-3-indolyl-β-D-galactoside) and S.O.C medium were purchased from Invitrogen. The purity of purified plasmids was analyzed by NanoDrop 1000 Spectrophotometer, and, then, the plasmids were sent for sequencing.

3.2.6 Sequencing and bioinformatics analysis of aptamers

Sequencing of a plasmid DNA of the selected transformants was done by automated DNA sequencing using ABI 3130xl analyzer Big dye 3.1 (ABI 7300 Sequence Detector, Foster City, CA, USA). Analysis of aptamer sequences nucleotide content, repeats and inverse complementary repeats were performed. For every selected aptamer, we computed all sites having mutually reverse complementary sequences and formed by three and more nucleotides. Sequence repeats within and between selected aptamers were computed as well. The secondary structures of sequenced aptamers were predicted by web-based OligoAnalyzer 3.1 tool from IDT (Integrated DNA Technologies, https://www.idtdna.com/calc/analyzer). Analysis of putative G quadruplex structures was carried out on a web-based server for predicting G quadruplexes in nucleotide sequences (http://bioinformatics.ramapo.edu/QGRS/analyze.php). The analysis of surface charges for MPT64 protein was based on data obtained from the protein database (RCSB Protein data bank). PDB database contained only one record 2HHI for *M. tuberculosis* MPT64 protein, resolved by solution NMR[79]. The electrostatic surface potential of 2HHI models was computed by DelPhi Web Server

(http://compbio.clemson.edu/sapp/delphi_webserver/) using AMBER parameters and Linear solver MPT64 2HHI model structure and accessible surface area and residues for the potential binding site were analyzed.

3.2.7 Detection of MPT64 with the ELONA

ELONA is a plate-based assay designed for the detection and quantification of complexes, where a protein is immobilized to a solid surface and, then, complexed with a biotinylated aptamer[149]. The complex is assessed by the absorbance change upon addition of a substrate (**Figure 3.1**). Seventeen identified aptamer sequences were further tested for their binding to the target MPT64 using ELONA based on protocol[150] with modifications. Non-target CFP-10 and ESAT-6 proteins were used as controls. Each biotinylated ssDNA used in the assay was custom synthesized (Sigma). Ninety-six-well plates (Bioster, A947978) were coated with 500 ng of protein in 100 µl of 100 mM Na_2CO_3 buffer overnight at 4 ^oC. After blocking with 1% BSA (Fisher Scientific, BPE1600-100) for 1 h at 4 ^oC the wells were washed 4 times with 1× TBS buffer (24.2 g Tris Base, 80 g NaCl, pH 7.6), and biotin-labelled ssDNA aptamers (500 nM) were added to each well and incubated for 2 h at 37 ^oC. The wells were then washed 4 times with 1× TBS buffer. Streptavidin-horseradish

peroxidase conjugate (Thermo Scientific, NE170004) was diluted in 1:10000 in TBS buffer and 100 µl was applied and incubated for 30 min at 37 ^oC. Then, a 50 µl of Turbo-3,3'5,5'-tetramethyl benzene (TMB, Sigma T8665) was added to each well and incubated for 15 min at 37 ^oC. The reaction was quenched by adding a 50 µl of 1 M H_2SO_4, and the protein-aptamer complex was quantified by determining the absorbance at 450 nm using MultiScan FC (Thermo Scientific) (**Figure 3.1**). In the background control, MPT64, CFP-10, and ESAT-6 were coated on the wells, but none of the ssDNA aptamers was added. For each sample, the optical density at 450 nm (OD) of the background was subtracted from the OD value of the experimental sample.

3.2.8 Determination of the Dissociation Constant (*K*$_D$) of aptamers

BIAcore X100 SPR instrument with SA chips (GE Healthcare, Vienna, Austria,) was used to determine the affinity of the ssDNA aptamer sequence (17) to MPT64 protein in kinetic studies. All experiments were conducted at 25 ^oC with a flow rate of 10 µl/min. HBS-EP buffer (0.01 M HEPES pH 7.4, 0.15 M NaCl, 3 mM EDTA, 0.005% v/v Surfactant P20) was

used as the running buffer and 12 mM NaOH (10 µl) was used as a regeneration buffer to remove the bound target. Selected biotinylated aptamers were immobilized onto the surface of the streptavidin

coated SA chip at a concentration of 1 µM for 10 min and followed by injecting 10 µM of biotin for 5 min and ethanolamine-HCl (1 M, pH 8.5) as blocking reagents. The flow cell with ethanolamine-HCl blocking, but without aptamer immobilization, was used as a control to subtract non-specific binding. MPT64 proteins with different concentrations (2.5, 5, 10, 20, and 40 µg/ml) were injected over the sensor chip, and the affinity binding was monitored for 2 min followed by washing with running buffer. The evaluation was done using the BiaEvaluation software (Biacore) by 1:1 [Langmuir] fitting model.

3.2.9 MPT64 antigen detection in sputum samples

A case-controlled study was performed to determine the specificity of aptamers with the highest binding capacity to MPT64. We obtained 43 sputum samples, 20 from patients with definite presence of *M. tuberculosis*, and 23 from non-tuberculous controls. Clinical samples were obtained from the regional Tuberculosis hospital (Astana, Kazakhstan). Patients were diagnosed with *M. tuberculosis* by phthisiatrician based on the criteria of Kazakhstani preventive measures on tuberculosis. The sputum samples from the hospital confirmed the presence of *M. tuberculosis* in infected patient samples using Ziehl–Neelsen stain and culturing at 37 ^{o}C in

Lowenstein-Jensen medium and Bactec MGIT for mycobacteria testing. Method of sputum liquefaction was same as in[151] with modifications. Briefly, 0.4 M NaOH solution was added into an equal volume of human sputum samples. The suspension was vortexed briefly. Subsequently, suspension from each tube was transferred to an empty tube, and 1 M HEPES buffer was added to each tube to neutralize the NaOH. The samples were then introduced onto the ninety-six well plates and left overnight at 4 ^{o}C. ELONA was performed to determine whether aptamer was able to detect the presence of MPT64 in sputum samples. The surface of microtiter plates was blocked using 1% BSA solution for 1 h at 4 ^{o}C. The wells were then washed 4 times with 1× TBS. Biotinylated aptamer sequences (16) and (17) in the concentration of 500 nM were added to each well and incubated for 2 h at 37 ^{o}C. In the background, control sputum samples were coated on the wells but none of the ssDNA aptamers were added. For each sample, the optical density at 450 nm (OD) of the background

was subtracted from the OD value of the experimental sample. ELONA results were then used for specificity and sensitivity comparison using 43 sputum samples, where each sputum sample was tested in a triplicate. The results were averaged, and the standard deviation was calculated for each sputum sample.

3.2.10 Data analysis

For ELONA assay, the OD values at 450nm were calculated by subtracting the background OD value and the data was presented in the form of Mean±SEM. One way analysis of variance was performed for aptamer sequence (17) to show the statistical difference as compared to control proteins. For SPR analysis, the K_D value was estimated by BiaEvaluation software (Biacore) using 1:1 [Langmuir] fitting model. The diagnostic value of the assay using aptamers on clinical sputum samples analysis was evaluated using Receiver Operating Characteristics (ROC) curve analysis (GraphPad Prism 6, Graphpad Software, Inc) based on interferential statistics. OD values were plotted and the area under the curves (AUC) and 95% confidence intervals (95% CIs), sensitivity and specificity values were calculated. The optimal cut-points were determined based on the maximum value of the Youden's index (YI=specificity+sensitivity-1).

3.3 Results and discussion

3.3.1 In vitro selection of aptamers

Theoretically, the DNA library used in this Chapter could potentially contain up to 4^{40} or 10^{24} different sequences, since the diversity of an oligonucleotide library is 4^n, where *n* is the length

of oligonucleotides[145]. However, in practice 10^{16} sequences are usually used[152]. Nevertheless, this is still much higher than possible murine antibodies of $10^9$to 10^{11}. This large range of sequences gives an opportunity to select ligands with a very high affinity[145]. The stability of aptamers in various temperature fluctuations offers another advantage, as they are tolerant of harsh chemicals and biological conditions as compared to antibodies. In addition to low-cost production and variability by modifications, aptamer in several studies showed to be extremely specific and sensitive being able to detect down to pM and fM range[113 153 154]. To achieve this concentration range, antifouling surface chemistry of aptamers on the surfaces needs to be carefully tuned and optimized for better detection and development of a sensitive aptasensor.

These parameters could greatly enhance both sensitivity and specificity of an aptasensor[113 154], where the detection limit could be lowered below the current clinical value detectionA random ssDNA library of about 10^{14} aptamers was screened for their efficiency to bind target MPT64. A commercially available MPT64 protein (Rv1980c) of *M. tuberculosis* H37Rv strain was used as the target. Following incubation, the bound oligonucleotides were separated from unbound ones via nitrocellulose filtration as described in the section 3.2.3 3 *"In vitro* selection of aptamers". Target-bound aptamers were eluted from the filters and enriched at each selection round by amplification using PCR. After each round of selection, the obtained DNAs were quantified by spectrophotometer and analyzed by PAGE gel. **Figure 3.2a** shows the PAGE gel of the 6th round of selection with an expected 80 bp DNA size. A total of ten rounds of repeated separation-amplification cycles were completed in order to receive a high affinity and specificity of MPT64 DNA aptamers.

Obtaining pure ssDNA is an important step during *in vitro* selection. We chose to use lambda exonuclease as it was shown to improve the SELEX efficiency and final purity of the ssDNA solutions, compared with the methods involving streptavidin-coated magnetic beads and further alkaline treatment[155].

As a rapid assessment, dot blot analysis was performed after SELEX rounds for evaluation of binding affinity to the target MPT64. In this regard, target MPT64 was spotted onto the nitrocellulose membrane in different concentrations, air-dried at room temperature, and then incubated with biotinylated aptamer pool from the 5th cycle. *E. coli* antibodies labelled with biotin served as a positive control, and deionized water served as a negative control. The results of the dot blot assay for the aptamer pool at the 5th cycle is presented in **Figure 3.2b**. Violet

stained spots on the nitrocellulose membrane (**Figure 3.2b**) indicated the binding reaction between the target protein and aptamer pool and developed a clear dot for the target MPT64 with a concentration of 87 µg/ml, while showed a faint dot for the concentration 8.7 µg/ml. With the increase of selection cycles, the selected aptamer pools showed stronger binding to the target with the increase of both dot size and intensity. Only after this confirmation, the next SELEX cycle was conducted. An affinity evaluation of obtained individual aptamers with known sequences was performed using the dot blot assay as well. Target protein in different

concentrations was immobilized on the surface of the nitrocellulose membrane, which was further incubated with biotinylated aptamer sequence (4). The amount of enzyme-linked conjugate bound was assayed by incubating the strip with an appropriate chromogenic substrate leading to colour development. Therefore, ssDNA aptamers were deemed to react with target protein when the strips showed purple dots. **Figure 3.2c** shows the dot blot affinity analysis for the aptamer sequence (4). The intensity of the violet stained spots increased with increasing concentrations of the selected aptamer (4), indicating that indeed the aptamer had an affinity to the target.

3.3.2 Sequencing and bioinformatics analysis

Cloning and sequencing of aptamer pools from ten rounds of SELEX cycles revealed seventeen aptamers with unique sequences. We further analyzed the sequences of aptamers (16) and (17) since they were the most specific to MPT64 as it was shown in an ELONA assay (**Figure 3.3b**). Computed GC/AT ratio (G+C)/(A+T) of all seventeen aptamers varies from 0.21 to 1.5, knowing that selected aptamer sequences (16) and (17) had GC/AT ratio of about 1.11. Aptamers (16) and (17) had the longest common TCCAGT sequence which was present once in each aptamer. The position of this sequence is similar in predicted secondary structures, based on Watson-Crick pairing A-T and G-C, for aptamers (16) and (17). In both aptamers, this sequence is located within the biggest potential stem-loop (hairpin), formed by four Watson Crick base pairs in stem parts and having 6/4 bases in loop part for aptamer sequences (17) and (16), respectively. In both aptamers (16) and (17), the GT suffix of this sequence belongs to the stem of the loop. Selected aptamer sequences did not have known G quadruplex motifs as found in anti-thrombin aptamer[156]. The GC/AT ratio is one of the basic sequence characteristics in terms of nucleotide composition and in future studies, aptamer sequences could be modified and optimized taking into account this ratio.

Surface charge analysis for the target MPT64 model (PDB code 2hhi) showed positively charged hydrophilic amino acids, such as arginine (ARG85 and ARG117) and lysine (LYS118), were found to be grouped allowing a potential binding site for the negatively charged DNA backbone.

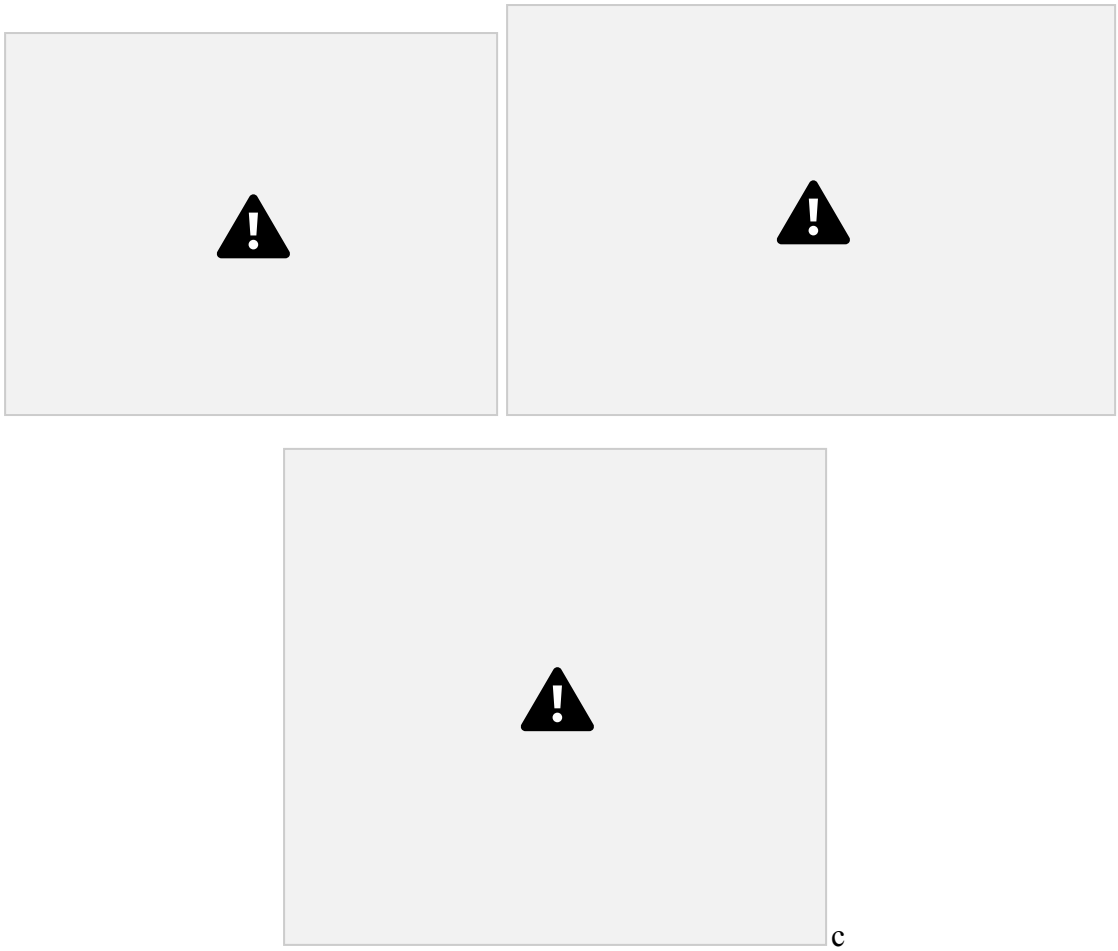

Figure 3.3 The binding affinity of selected ssDNA aptamers to proteins MPT64, ESAT-6, CFP 10. Binding of biotinylated ssDNA aptamers to the target MPT64, and non-target ESAT-6 and CFP-10 was determined by an ELONA assay. Binding of the ssDNA aptamers to ESAT-6 and CFP-10 is shown for comparative purposes. **(a)** Individual aptamer sequences (1-17) (500 nM) were incubated in wells coated with target MPT64, and non-target ESAT-6 and CFP-10. Aptamers (17) are shown in circles. All data are shown in the form of Mean±SEM. (n=6) **(b)** ELONA analysis of the relative binding abilities of individual aptamer sequences (1-17). **(c)** Binding of the aptamer sequence (17) to the target MPT64. All data are shown in the form of Mean±SEM (n=3).

3.3.3 Evaluation and characterization of DNA aptamers

ELONA was used to determine the binding interaction between the selected aptamer sequences and the target MPT64. Non-target *M. tuberculosis* immunogenic secreted proteins ESAT-6 and CFP-10 with a concentration of 500 ng/ml were also tested to check any cross-reactivity.

Experiments were conducted in six replicates. A general pattern shows that all aptamers have higher binding to the target MPT64 compared to non-target ESAT-6 and CFP-10 (**Figure 3.3a, Figure 3.4**). **Figure 3.3a** shows the values with error bars in grouped format whereas, **Figure 3.4** shows the values with error bars for individual aptamer sequences. One way analysis of variance for aptamer sequence (17) (**Figure3.3a** presented in red circles) for target and non target proteins, showed that that the P value was 0.0004 indicating the statistical significant difference. ELONA analysis of the relative binding abilities of individual aptamer sequences (1-17) was further calculated. This was done by simply subtracting the mean absorbance value of MPT64 - aptamer complex (from **Figure 3.4**) by the highest mean absorbance value of either aptamer-ESAT-6 or aptamer-CFP-10 complexes (**Figure 3.3b**). No error bars can be calculated from this subtraction. The negative value for aptamer sequence (10) shows that the oligonucleotide preferentially binds to either ESAT-6 or CFP-10 and not to target MPT64. As the result aptamer sequence (17) showed the highest binding to target MPT64 rather than to non-target proteins used in this assay (**Figure 3.3b, Figure 3.4**). Therefore, the aptamer sequence (17) was chosen for further assessment. The dose-response analysis for the aptamer sequence (17) showed an increase in absorbance signal from concentration ranging from 12 nM to 250 nM. There was no further increase observed after 250 nM indicating that the surface was saturated above this concentration (**Figure 3.3c**). A linear correlation was found between OD_{450} value and aptamer sequence (17) in a range of concentration (**Figure 3.3c**). The regression equation for OD_{450} difference versus aptamer (17) concentration was $y=0.1436x+0.056$ with $R^2 = 0.94$, where x is the concentration of aptamer sequence (17) in nM (**Figure 3.3c**). The result showed that the selected aptamer could be used as a recognition ligand to detect target MPT64.

SPR is a technique used to follow the dynamics of interactions between a target molecule immobilized on a biochip and a ligand introduced in a solution. It allows apparent kinetic constants to be estimated for the formation of a specific complex and a quantitative estimation of the affinity of the ligand for the target molecule to be calculated. In general, an SPR technique comprises of one probe (for example ssDNA aptamer probe specific to MPT64) which is immobilized on the SPR chip **(Figure 3.5 a)** and the analyte (for example MPT64 protein)

solution flowed over the chip surface at a certain flow rate. The main component in the detection of this technique is based on surface plasmon resonance- an electromagnetic wave

associated with longitudinal oscillation of the free electrons at the interface of the metal and the dielectric, which is extremely sensitive to the variation of the refraction index within the first 200 nm from the biochip surface[157]. The collective oscillations of free electrons also known as surface plasmons are excited and detected via the Kretschmann configuration, in which light is focused onto a metal film through a glass prism and the subsequent reflection is detected[158]. At a certain incident angle, the plasmons resonate with light, resulting in the absorption of light which creates a dark band line in the reflected beam (**Figure 3.5a**). That dark band line can be observed as a dip in SPR reflection intensity. A shift in the reflectivity curve represents a molecular binding event taking place either on or near the metal film, or a conformational change in the molecules bound to the film[157]. By monitoring this shift *vs*. time, molecular binding events can be studied.

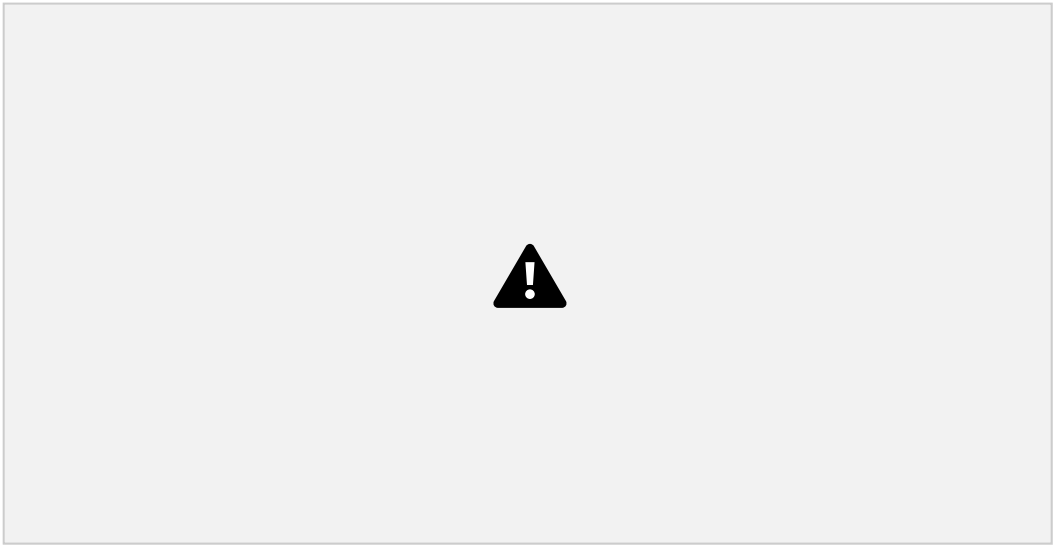

Figure 3.4

The binding affinity of selected ssDNA aptamers to proteins MPT64, ESAT-6, CFP 10. Binding of biotinylated ssDNA aptamer candidates to target MPT64, and to non-target ESAT-6 and CFP-10 was determined by ELONA. Binding of ssDNA aptamers to non-target ESAT-6 and CFP-10 is shown for comparative purposes. Aptamer sequences (1-17) (500 nM) were incubated in wells coated with proteins MPT64, ESAT-6 and CFP-10. All data are shown in the form of Mean ± SEM (n=6).

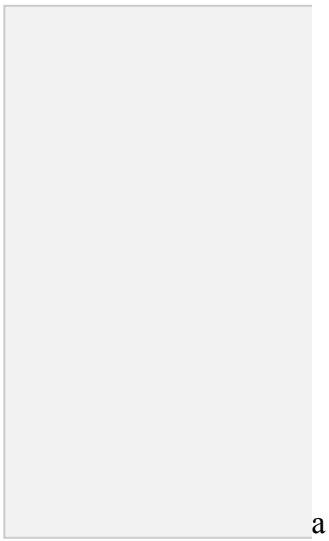

a

b **Figure 3.5 (a)** Schematic representation of SPR. P-polarised light is directed to the high refractive index prism (in contact with the streptavidin coated SA chip), on which the biotinylated aptamer is attached. The output signal in the form of the reflected light is then represented as resonant unit variations vs time upon protein (MPT64) binding. (b) An overlay of the SPR signals from the interaction between the target MPT64 and aptamer (17). In each

case, MPT64 was injected over immobilized aptamer (17) with an initial concentration of 2.5, followed by 5, 10, 20, and 40 μg/ml.

In this Chapter, SPR was used to identify the affinity of the selected aptamer sequence (17) against target MPT64. Immobilization of the aptamer was based on streptavidin-biotin interaction. SPR signal reached 1510.8 RU after injecting a biotinylated aptamer over a sensor chip coated with streptavidin, indicating immobilization of the aptamer on the sensor surface via biotin to streptavidin interactions. MPT64 protein at different concentrations (2.5, 5, 10, 20, 40 μg/ml) was injected onto the sensor chip so the association and dissociation of the complex could be monitored as a function of time. The protein was injected at increasing concentrations

over the aptamer coated surface and the reference was taken directly on the surface without aptamer. The analytical signal was computed as the difference between the signals (resonance units, RU) detected on the aptamer surface and on the reference. An overlay of the SPR signal from the interactions between aptamer (17) and the target MPT64 is shown in **Figure 3.5b**. With increasing MPT64 concentrations there was also an increase in RU. The calculated k_a (association rate constant) for aptamer sequence (17) was 9.93×10^{-4} ($M^{-1}s^{-1}$) and K_D (dissociation rate constant) was 8.85×10^{-4}(s^{-1}) and K_D (dissociation equilibrium constant) was 8.92 nM. The K_D in nanomolar rage indicates a tight affinity to the MPT64 protein[159]. The binding kinetics of the immobilized ssDNA aptamers to MPT64 protein was determined using BiaCore X100 surface plasmon resonance.

3.3.4 MPT64 antigen detection in sputum samples

Forty-three sputum samples were used to evaluate aptamer sequences (16) and (17) for detecting TB infection in a case-controlled study using ELONA. Aptamer (16) was the second in line for specific MPT64 binding, and it was used for comparison purposes. It was found that OD_{450} values were significantly higher in those patients with active TB than in TB (-) individuals (**Figure 3.6a,** $p \leq 0.0001$). Twenty of sputum samples had a confirmed TB and twenty-three samples were obtained from TB (-) individuals. The specificity and sensitivity of the sputum sample analysis based on aptamer (17) by ELONA were calculated as 90% (96 CI: 68.3-98.7%) and 91.3% (95% CI: 71.96 - 98.93%), respectively, using Youden's index. The AUC was 94.78% (95% CI: 89-100%) from the ROC curve (**Figure 3.6b**). The specificity and sensitivity for aptamer (16) was 75% (95% CI: 50.9-91.34%) and 100% (95% CI:

85.75-100%), respectively. The AUC for aptamer (16) was 95% (95% CI: 89.37-100%) (**Figure 3.6c**).

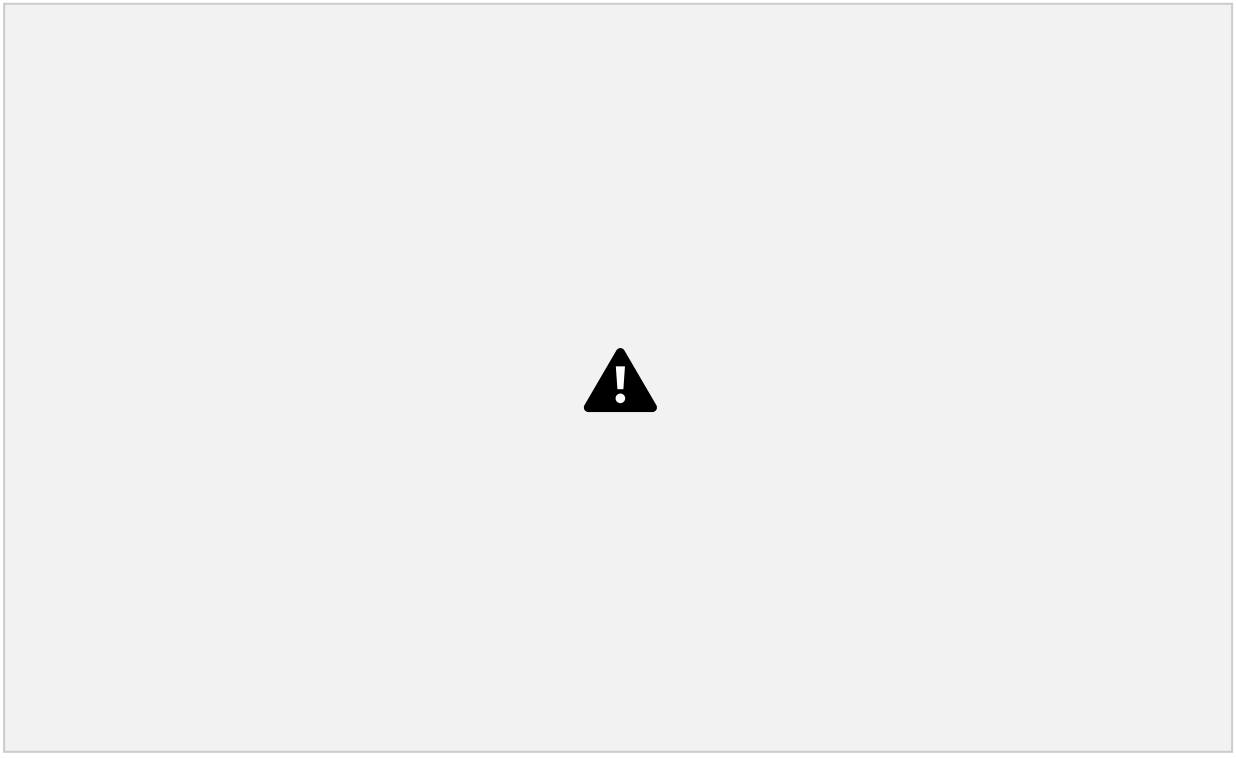

Figure 3.6 Detection of MPT64 antigens in sputum samples. **(a)** ELONA based assay for the detection of MPT64 antigens in TB infected and TB (-) using aptamer sequences (16) and (17); **(b, c)** The ROC curve of aptamer sequences (17) and (16), respectively, based on ELONA.

3.4 Summary

In this Chapter, aptamers against *M. tuberculosis* secreted protein MPT64 were successfully selected and could be used as an alternative for the detection and diagnosis of TB for infield or on-site application. The selected aptamers showed good specificity and sensitivity values;

therefore, they would likely be less prone to give false positive results. The selected aptamer could also be used in a multiplexed assay for TB diagnosis alongside with other aptamers selected against ESAT-6, CFP-10, and surface saccharides of *M. tuberculosis*. The previous study with ESAT-6 and CFP-10 showed that the binding of some aptamers could be abrogated by the presence of anti-MPT64 antibody by possibly competing to the same binding site[150]. In addition, due to the steric hindrance and the size difference between aptamer and antibody, the information obtained from ELONA i.e. absorbance value would be different as well. Therefore, the current study did not compare the binding process of aptamer-MPT64 with that of antibody MPT64. The comparison could be done after optimizing the surface chemistry for aptamer and measuring the values using different techniques, such as electrochemical impedance spectroscopy (EIS). In case of the low signal, aptamers could be modified easily such as

labelling with magnetic/gold nanoparticles or with fluorescent reporting molecules, which offer great potential for the development of aptamer-based detection technologies for rapid, cost effective and reliable detection method for TB diagnosis. Additional NMR, colourimetry studies, and further bioinformatics analysis and aptamer manipulation could be conducted for improved aptasensor applications. For future studies, the specificity and sensitivity test could be validated by testing sputum samples from chronic patients with no TB infection, such as asthmatic.

In conclusion, selected ssDNA aptamer bounded specifically to the target MPT64 using the SELEX technology. Selected aptamers further showed a strong binding affinity with high specificity against *M. tuberculosis* secreted protein MPT64. Following Chapters will focus on optimizing the surface chemistry for the development of an aptasensor using the selected aptamers as bio-recognition elements for the TB diagnosis.

Chapter 4. Optimization and development of a sensitive electrochemical aptasensor for the detection of MPT64 in human serum

This Chapter provides a presentation on the optimization of surface chemistry using the selected aptamers and the development of an aptasensor for the detection of MPT64. The study focuses on EIS as a detection technique and Bio-FET, as a validation tool. The chapter highlights the effect of buffer conditions on the EIS signal, the effect of anti-MPT64 DNA aptamer surface density on MPT64 binding efficiency, the transition from 6-mercapto-1-hexanol (MCH) to thiol terminated triethylene glycol mono-11-mercaptoundecyl ether (EG) based self-assembled monolayer (SAM) for enhanced antifouling properties.

The work presented in this Chapter was published in[2].

4.1 Abstract

In the previous chapter, an aptamer against MPT64 with the dissociation equilibrium constant K_D of 8.92 nM was selected using the SELEX technique, which was also tested for its specificity on clinical sputum samples[160]. This Chapter reports on the development of an aptasensor for the detection of MPT64 in blood serum by utilizing a previously selected aptamer against MPT64 and exploring in detail the effect of the surface chemistry and aptamer linker molecule type on the aptasensor performance. The binding performance of an aptamer to the target is highly dependent on a type of a linker between the aptamer and the surface and also a co-adsorbent[161]. The type of co-adsorbent influences a considerable reduction of non-specific binding while maintaining the integrity of the immobilized biomolecules[162]. This chapter investigates the combinatorial effects of the aptamer linker and a co-adsorbent onto gold electrodes for optimal binding efficiency and reduced non-specific interactions for label-free detection using electrochemical impedance spectroscopy. Two types of co-adsorbents and two types of aptamer linkers were studied and high specificity and sensitivity to MPT64 was observed for a surface prepared with a 100 µM of thiol PEGylated aptamer HS-$(CH_2)_6$-$OP(O)_2O$-$(CH_2CH_2O)_6$- TTTTT-aptamer and 100 µM of 6-mercaptohexanol in a ratio of 1:100. The developed aptamer based sensor was successfully used with spiked human serum samples with a limit of detection of 81 pM. The work presented in this chapter demonstrates the use of an aptamer as a lower cost, more sustainable and more stable alternative of antibodies for the development of point of-care tuberculosis aptasensors decreasing the detection time from several days and/or hours to 30 min.

4.2 Material and methods

4.2.1 Reagents

Thiolated MPT64 aptamers in the form of HS-$(CH_6)_6$-$OP(O)_2O$-$(CH_2CH_2O)_6$-5'-TTTTT aptamer-3' (24.3 nmol) were synthesized by Eurogentec (Belgium), and HS-$(CH_6)_6$-5'-TTTTT aptamer-3' (47.4 nmol) were synthesized by Sigma Aldrich (UK). Phosphate buffered saline (PBS, 0.01 M, pH 7.4) tablets, human serum albumin (HSA, lyophilized powder, ≥ 97%), human serum (from human male AB plasma), trizma base (≥ 99.0%), hydrochloric acid (HCl, 37%), magnesium chloride ($MgCl_2$, powder, < 200 µm), sodium chloride (NaCl, ≥ 99.5%), sulfuric acid (H_2SO_4, 1 M), ethylenediaminetetraacetic acid (EDTA, 0.5 M in H_2O, pH 8),

triethylene glycol mono-11-mercaptoundecyl ether (EG), potassium hexacyanoferrate (III), potassium hexacyanoferrate (II) trihydrate, hexaammineruthenium (III) chloride ($Ru(NH_3)_6^{3+}$, 98%) and 6-mercapto-1-hexanol (MCH) used in the sample preparation were of analytical grade and purchased from Sigma-Aldrich, UK. Isopropanol (propane-2-ol, HPLC grade), absolute ethanol (HPLC grade) were purchased from Fisher Scientific. An electrode polishing kit was obtained from BASi Inc. (Japan). MPT64 protein (E5-00061, 1 mg) was purchased from EnoGene (China). Prostate-specific antigen (PSA, 100 μg) and carcinoembryonic antigen (CEA, 1 mg) were purchased from Calbiochem (Canada) and USBiological (USA), respectively. All aqueous solutions were prepared using 18.2 MΩcm ultra-pure water with a Pyrogard filter (Millipore, UK).

4.2.2 Apparatus

Measurements were recorded using a CompactStat potentiostat (Ivium Technologies, the Netherlands) with Ivium soft Electrochemistry software. A three-electrode cell with an Ag/AgCl reference electrode (BASi, USA) connected via a salt bridge filled with a buffer and platinum counter electrode (ALS, Japan) was used for all measurements. The electrochemical impedance spectrum was measured in a buffer containing 2 mM ferro/ferricyanide $[Fe(CN)_6]^{3-/4-}$ redox couple (potassium hexacyanoferrate II/III). The frequency range used for the measurement was in the range of 10 kHz to 100 MHz, with a 10 mV a.c. voltage superimposed on a bias d.c. voltage of 0.2 V *vs.* Ag/AgCl, corresponding to the formal potential of the redox couple. All measurements were performed at room temperature inside a Faraday cage. All measurements were carried out in triplicate, and the mean value of replicates, standard deviations and standard errors from the mean were used to report the results.

4.2.3 Electrode surface preparation

Gold disk working electrodes with 2 mm diameter (CH Instruments, TX, USA) were cleaned mechanically and electrochemically. Electrodes were first cleaned by sonication in absolute ethanol for 10 min, then mechanically polished for 2 min with 1 μm diamond powder and finally with 0.05 μm alumina slurry on respective polishing pads. The electrodes were sonicated for 2 min in isopropanol and for 10 min in Milli-Q water after each step. Electrodes were then cleaned electrochemically in 0.5 M H_2SO_4 by scanning the potential between oxidation and reduction of gold, -0.05 and 1.1 V *vs.* Ag/AgCl for 50 cycles. The electrodes were then thoroughly rinsed with Milli-Q water and air dried.

4.2.4. Co-adsorbent and DNA immobilization

For the development of the MPT64 aptasensor with a co-adsorbent (either MCH or EG), gold disk working electrodes were incubated for 16 h at 4 °C with a 150 µl mixture of 100 µM of DNA aptamer (either short linker or long linker) and 100 µM of co-adsorbent, mixed in different ratios. This step was important for an aptamer immobilization on the surface via disulphide bonds. The combination of an aptamer and a co-adsorbent used in this study is presented in **Figure 4.1**. Both MCH and EG were initially diluted in absolute ethanol at 100 mM to make a stock solution and stored at -20 °C. Further dilutions of both MCH and EG were prepared prior to incubation in different measurement buffers: SELEX buffer (50 mM Tris-HCl; 25 mM NaCl; 5 mM $MgCl_2$; pH 7.5), 10 × diluted SELEX buffer, PBS buffer (10 mM and/or 1 mM, pH 7.4). All buffer solutions were filtered using a non-pyrogenic sterile polystyrene 500 ml bottle top filter (Corning Incorporated) and adjusted at room temperature before use. Prior to mixing with the co-adsorbents, the DNA aptamer was heated for 5 min at 95 °C and slowly cooled down to room temperature. This step was important to linearize the aptamer sequence and slowly allow it to obtain its favourable conformation. After incubation, the electrodes were rinsed with measurement buffer to remove any unattached DNA aptamers. 150 µl of 1 mM of either MCH or EG was applied onto the surface of the electrodes for another 1 h at room temperature to ensure complete thiol coverage of the gold surface and to displace non-specific interactions between the DNA and gold[113 135]. After rinsing the electrodes with the measurement buffer, they were placed into the measurement buffer with 2 mM ferro/ferricyanide $[Fe(CN)_6]^{3-/4-}$ redox couple for at least 1 h for the surface stabilization until a stable EIS signal was obtained. The stability measurements were performed in the same time interval that was used for incubation

with protein to monitor the drift over time or any changes in EIS due to external factors. Once stable Nyquist curves were recorded, only the proteins were incubated to monitor binding events. The stability of the signal was an indicator of the fact that the aptamer had stable conformational change on the electrode surface with no further fluctuations in the EIS signal. The stable signal was used as a reference for subsequent protein concentration measurements.

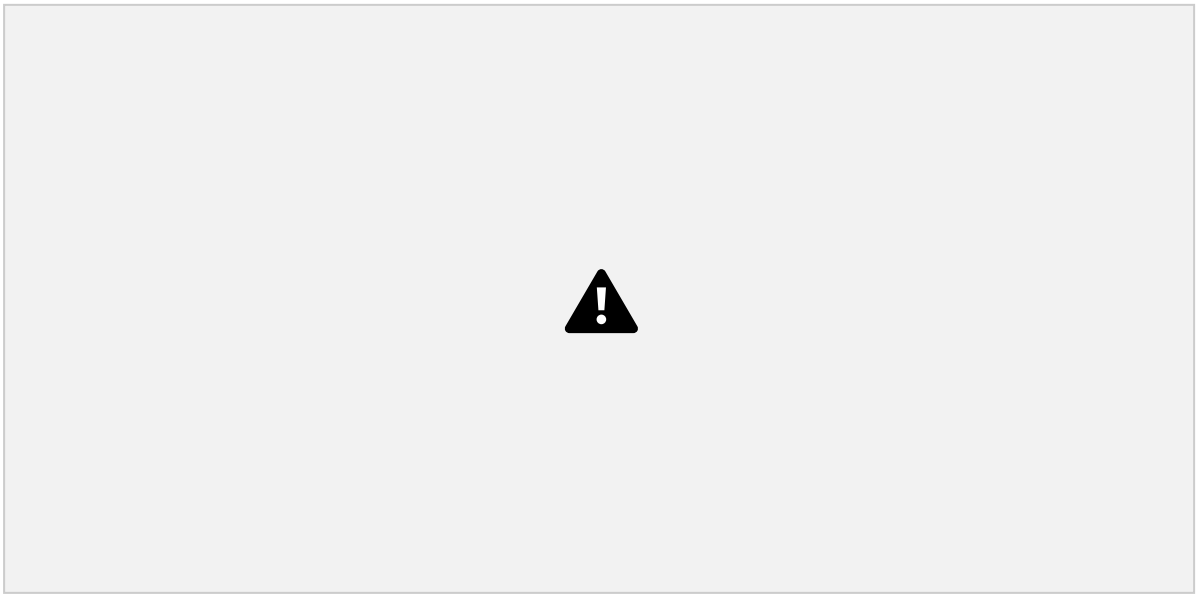

Figure 4.1 An aptasensor surface modification based on different chemistries applied onto the gold surface of the electrode; (a) short linker DNA aptamer/MCH; (b) long linker DNA aptamer/EG; (c) long linker DNA aptamer/MCH.

4.2.5 Detection of MPT64

Detection of the target MPT64 with the electrochemical aptasensor was achieved by incubating the co-adsorbent and DNA immobilized electrodes in the solution containing target MPT64 for 30 min at room temperature. For the detection studies, a wide range of MPT64 concentrations were used from 24 pM up to 200 nM. MPT64 protein was diluted in different measurement buffers: SELEX buffer; 10× diluted SELEX buffer; 10 mM PBS; 1 mM PBS; 1/10 and 1/100 diluted human serum samples in SELEX buffer.

For the specificity studies different concentrations (0.1, 1, and 10 nM) of non-target proteins HSA, CEA, PSA, and target MPT64 protein diluted in SELEX buffer were incubated for 30 min

on the gold electrode surface based on a long linker DNA aptamer/MCH surface chemistry at a ratio of 1/100.

4.2.6 Preparation and measurement of spiked samples with MPT64 Serum samples were

filtered using a 0.2 µm sterile syringe (Corning Inc., NY, USA) to remove large molecular formations. The serum dilutions (1/100 and 1/10) were made in SELEX buffer. Co-adsorbent and DNA immobilized electrodes were first stabilized in diluted serum for at least 1 h until a stable signal was recorded from the EIS measurement. The electrodes were then incubated in diluted serum with a wide range of MPT64 protein concentrations (from 24 pM up to 100 nM) for 30 min at room temperature.

4.2.7 BioFET measurements

Biologically-sensitive field-effect transistors (BioFETs) were used to confirm the EIS results. The BioFET measurements were carried out in an extended gate mode by connecting the gold electrodes via a metal wire to the gate of an n-type metal oxide semiconductor field-effect transistor (MOSFET)[112]. The MOSFET readings were recorded using an Agilent B1500A Semiconductor Device Analyzer with EasyEXPERT software. The sensor consisted of thin film gold electrodes (Micrux Technologies, Spain) placed in a flow cell. The FET structure was used to transduce the binding events on the gold electrode into a shift in the threshold voltage of the transistor. An Ag wire coated with silver chloride paste (ALS, Japan) served as a reference electrode. Prior to a co-adsorbent/aptamer complex immobilization, electrodes were cleaned by sonication in absolute ethanol for 5 min and then in ultrapure water for an additional 5 min. The electrode surface preparation was the same as described in section 4.2.4 "Co-adsorbent and DNA immobilization", but without the use of redox markers. Different concentrations (0.001, 0.01, 0.1, and 1 nM) of MPT64 were diluted in SELEX buffer and measured using the same conditions as performed for EIS measurements.

4.2.8 Contact angle measurement

An in-house built optical angle setup was used for contact angle measurement after each immobilization and detection steps[163]. Due to the inability of the setup to accommodate the measurement electrodes, thermally evaporated gold electrodes were used instead. The electrodes were sonicated in absolute ethanol for 5 min and then in ultrapure water for another 5 min. Electrodes were then exposed to UV/ozone for 30 min. The MCH/aptamer complex was

prepared and incubated overnight as described in section 4.2.4. "Co-adsorbent and DNA immobilization". 50 nM of MPT64 was applied onto the pre-treated surface of the electrode for 30 min, and 50 nM HSA served as a control. Electrodes were then rinsed with ultrapure water

and dried under a gentle air flux. Electrodes were then placed on the stage and a 5 µl drop of ultrapure water was dispensed. The wetting of surface was then captured using a Nikon p520 camera. The contact angle was measured using an on-screen protractor GNU GPL v3 (http://osprotractor.sourceforge.net/Protractor.html).

4.2.9 Chronocoulometry

The surface density of DNA aptamer immobilized on the electrode was determined using chronocoulometry[135 164 165]. The method was used to determine the optimal ratio for MPT64 detection on the electrode surface at different ratios of a long linker aptamer/MCH (1/50; 1/100; 1/200; 1/500) required for MPT64 binding. The final thiol concentration was adjusted to 100 µM. Electrodes functionalized with DNA aptamer and MCH were first immersed into 10 mM Tris-HCl (pH 7.4) for 1 h. A potential step from -300 to -800 mV vs Hg/Hg_2SO_4 was applied for 500 ms, and the resulting charge flow was measured. The same electrodes were then immersed into 100 µM hexaammineruthenium (III) chloride ($Ru(NH_3)_6^{3+}$) in 10 mM Tris-HCl (pH 7.4) buffer, and the resulting charge was again measured. The number of aptamer molecules per electrode area was calculated based on the integrated Cottrell equation[135]. The DNA surface density was determined from the surface excess of $Ru(NH_3)_6^{3+}$ as $\Gamma_{DNA} = \Gamma_0(z/m)N_A$, where Γ_{DNA} is the probe surface density (molecules/cm^2), m is the number of negatively charged phosphate groups on the probe DNA, z is the charge on the redox molecule, and N_A is Avogadro's constant. The number of DNA molecules for each long linker aptamer/MCH ratio was calculated as the mean of three different electrodes based on the Cottrell equation presented above. For the protein binding studies, the $Ru(NH_3)_6^{3+}$ molecules were removed from the previously used electrodes by incubating and gently shaking the electrodes in 10 mM Tris-HCl with 10 mM EDTA pH 7.4 for 15 min. The electrodes were then rinsed with the measurement buffer and stabilized for at least 1 h in measurement buffer with 2 mM ferro/ferricyanide $[Fe(CN)_6]^{3-/4-}$ redox couple followed by the EIS measurement. The electrodes were then immersed in different concentrations of MPT64 protein (0.1, 1, 10 nM) for 30 min followed by rinsing with measurement buffer, which was then ready for a new EIS measurement recording.

4.2.10 Data analysis

All data analyses were performed using GraphPad Prism 6 (Graphpad Software, Inc), Origin

Pro (OriginLab Corporation), and Excel (Microsoft Office Professional Plus 2013). All data was presented in the form of Mean ± SEM of three replicates. The number of aptamer molecules on each electrode surface was calculated using the formula $\Gamma_{DNA} = \Gamma_0(z/m)N_A$, where Γ_{DNA} is the probe surface density (molecules/cm^2), m is the number of negatively charged phosphate groups on the probe DNA, z is the charge on the redox molecule, and N_A is Avogadro's constant. The R_{ct} signal change was calculated based on the values obtained from fitting circuit. The descriptive statistics was used to analyze the data for surface chemistry optimization, chronocoulometry, BioFET experiments. The descriptive and interferential statistical analysis was carried for EIS experiments and contact angle measurement experiment. The linear correlation curve with regression equation was used to correlate R_{ct} change at different target protein concentrations. The statistically significant difference of the P value between the means of each functionalization step in contact angle measurement experiments was determined using one-way analysis of variance.

4.3 Results and discussion

4.3.1 Surface chemistry optimization studies

The type and the length of the aptamer linker and co-adsorbent were shown to be important for the aptasensor development[161]. **Figure 4.1** presents a schematic overview of the sensor surface chemistries applied in this study, which includes three different types based on either DNA aptamer with a short or long linker and MCH and EG as a co-adsorbent. Based on other published work[162] on antifouling properties of aptamer with the linker and the EG, we did not test the combination of short linker DNA and EG as a co-adsorbent. This combination could hinder or diminish the availability of the short linker aptamer to the MPT64 and make the aptamer inaccessible and/or unavailable to the MPT64 protein.

Chapter 3 reported a study on selection, characterization, and application of DNA aptamers for the detection of *M. tuberculosis* secreted protein MPT64, where aptamers were selected using the SELEX method and tested on clinical sputum samples using ELONA with sensitivity and specificity of 91.3% and 90%, respectively[143]. The total length of the DNA aptamer was 40 nucleotides, which was modified in this study by the addition of the long linker in the form of

HS-$(CH_2)_6$-$OP(O)_2O$-$(CH_2CH_2O)_6$-TTTTT-aptamer and the shorter linker HS-$(CH_2)_6$-TTTTT

aptamer. The $(CH_2)_6$ linker and five thymine residues were included to provide spacing between the aptamer and the surface so that it can easily fold and capture the protein. The long linker was made of additional ethylene oxide $(CH_2CH_2O)_6$, a hydrophilic part of the linker. This group is essential for protruding the aptamer from the monolayer surface and, thereby, avoiding any steric hindrance associated with protein binding. The ethylene oxide also reduces non-specific binding on the electrode surface[166] [167]. Both MCH and EG are simple and common chemicals that were used as a co-adsorbent for the modification of surfaces and were used for the detection of molecules.

To determine which surface chemistry would provide better binding to our protein of interest, the BioFET was recorded after incubating the electrode surface with the target MPT64 (**Figure 4.2a**). The BioFET allows the immobilization of an aptamer layer onto an extended gate of a MOSFET and enables fast quantification of an electrical charge variation arising from protein binding. With the BioFET technique, very low limits of detection can be obtained and, hence, can be used to confirm results obtained from EIS. **Figure. 4.3b** illustrates a typical transfer characteristic (drain current, I_D, *vs.* gate-to-source voltage, V_{GS}) curve for an electrode before and after MPT64 binding event onto the surface of the functionalized gold electrode. Depending on the surface charges of the protein, the BioFET can produce a positive or negative shift in its transfer characteristic. Any changes in V_{GS} modulate the conductivity of the channel and thereby alter the drain current[112]. Surface charge analysis for MPT64 previously showed that positively charged hydrophilic amino acids, such as arginine and lysine, were found to be grouped on the surface of the protein. Hence, the positive charge of MPT64 produced a negative shift in the V_{GS} of the BioFET as can be seen in **Figure 4.2b**. **Figure 4.2c** presents the values of ΔV_{GS} for different MPT64 concentrations (0.001, 0.01, 0.1, 1 nM) on different surface modifications onto the thin film gold electrode: (i) a short linker aptamer/MCH, (ii) a long linker aptamer/EG, and (iii) a long linker aptamer/MCH. The ΔV_{GS} for all three surface chemistries was determined at I_D=22.5 µA. The ΔV_{GS} for the long linker aptamer/MCH complex increased from -17.35 mV to -42.13mV when the MPT64 concentration increased from 1 pM to 1 nM. The combination of the two other surface chemistries (long linker DNA aptamer/EG and short linker DNA aptamer/MCH) studies showed inconsistent changes in ΔV_{GS} (**Figure. 4.2c**) with large error bars. This inconsistency could be due to a non-specific binding of the target protein on the functionalized surface and reduced reproducibility. The BioFET data suggests that the surface

chemistry based on the long linker DNA aptamer/MCH (**Figure 4.1c**) would provide better antifouling properties for MPT64 binding, better reproducibility, as well as improved specificity towards the protein detection.

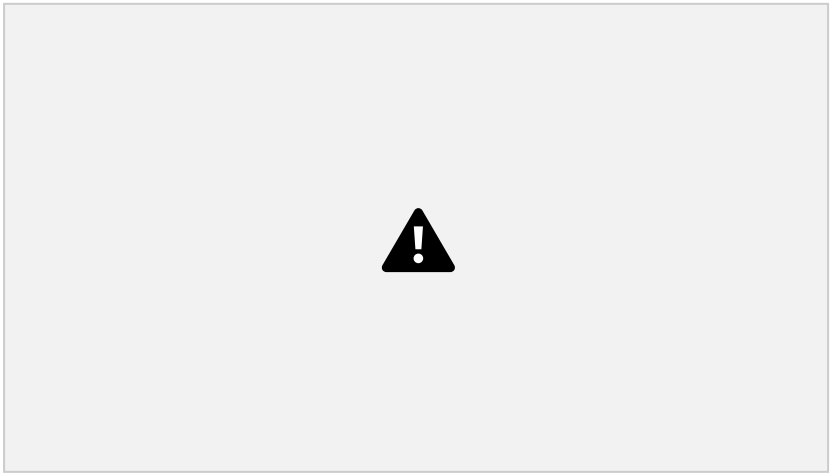
a

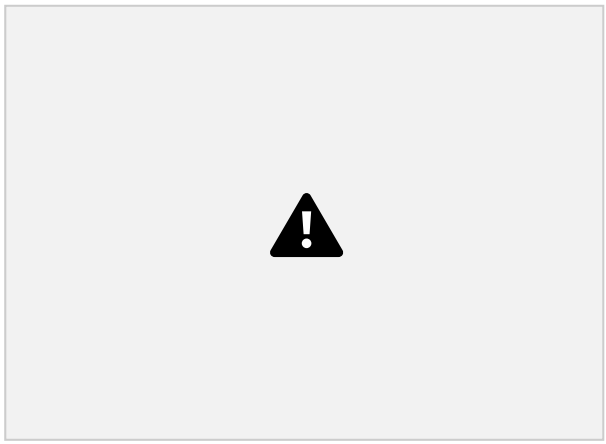

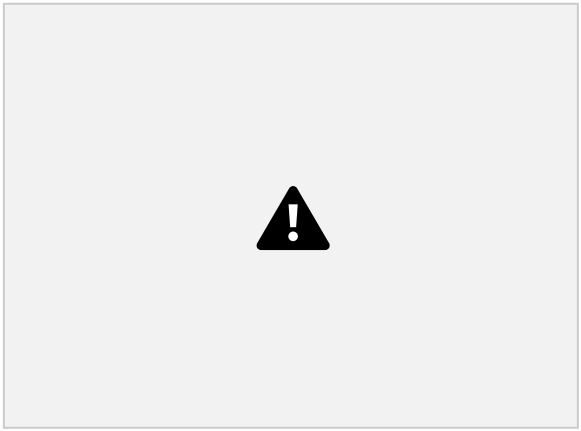
b

c

Figure 4.2 Target MPT64 detection using BioFET. (a) A schematic representation of BioFET set-up; (b) A typical I_D/V_{GS} characteristic curve for an electrode before (solid line) and after (dashed line) MPT64 binding event based on a long linker aptamer/MCH complex; (c) V_{GS}

changes on the surface of the electrode upon incubation with different MPT64 concentrations in SELEX buffer based on a short linker aptamer/MCH (1/100 ratio), long linker aptamer/EG (1/100 ratio), and long linker aptamer/MCH (1/100 ratio). All measurements were recorded on three separate electrodes.

The EIS signal was also recorded for the three surface chemistries: a short linker DNA aptamer/MCH, a long linker DNA aptamer/MCH, and a long linker DNA aptamer/EG. The

surface chemistry based on a short linker-DNA aptamer/MCH (**Figure 4.1a**) showed a concentration-dependent increase in charge transfer resistance R_{ct} change (3.9%, 7.5% and 13.3% at 0.1, 1, and 10 nM of MPT64, respectively) (**Figure 4.3**). The same surface chemistry showed a non-specific interaction with HSA (with an R_{ct} change between 2.3% at 0.1 nM and 12.3% at 10 nM). The results for this specific surface chemistry showed that the short linker aptamer/MCH approach, although sensitive to MPT64, does not prevent the binding of interfering molecules, hence making it an unreliable surface for use with complex samples. In addition, the large error bars in **Figure 4.3** are indicative of electrode to electrode variability. The surface chemistry based on the long linker DNA aptamer/MCH (**Figure 4.1c**), measured with redox markers in solution, showed a R_{ct} signal change that increases with MPT64 concentration (5.8%, 12.0% and 21.2% for 0.1, 1, and 10 nM of MPT64, respectively), whereas it remained almost unchanged (less than 4%) when incubated with HSA up to a concentration of 10 nM (**Figure 4.3**). These measurements were recorded upon a 1/100 ratio of long linker DNA aptamer/MCH. This significant increase in R_{ct} signal from 5.8% up to 21.2% for MPT64 compared to other surface chemistries studied could be due to the blocking effect to electron transfer after attachment of protein onto the surface of the modified electrode. Another reason could be due to the extended nature of the aptamer that forms a brush like conformation, which protrudes from the short MCH monolayer[162]. Thereby, the freely moving extended nature of the aptamer with the long linker enabled MPT64 to bind more efficiently compared to other surface chemistry studies and reduced non-specific binding. The long linker-DNA aptamer/EG based surface chemistry (**Figure 4.1b**) promotes the formation of an insulating surface, not suitable for Faradaic measurements. Therefore, measurements were conducted without the use of the redox probes (i.e. in a non-Faradaic mode) to evaluate the capacitive processes on the surface. A complex capacitance was calculated and used in order to evaluate the capacitance from the impedance data[135]. The

signal at the beginning of the recording was quite unstable and no significant changes were observed in the capacitance upon MPT64 binding (**Figure 4.4**). In order to evaluate the capacitance of the system, a complex capacitance was defined as:

$$C^{*} = -\frac{Z''}{\omega |Z|^{2}} - \frac{Z'}{\omega |Z|^{2}} = C' + C'' \quad (6)$$

where C' corresponds to the real part of the capacitance, and C'' corresponds to the imaginary part of the capacitance. Z' and Z'' are the real and imaginary components of the measured impedance, respectively, and $\omega = 2\pi f$ is the angular frequency of the measurement. From the

capacitance data, Cole-Cole capacitance plots can be obtained. With these plots, the diameter of the obtained semicircle corresponds to the capacitance of the system. **Figure 4.4** depicts an example of the non-Faradaic EIS measurement of the electrode modified with the long linker DNA aptamer/EG based surface chemistry upon MPT64 binding. Although there is significant noise at high frequencies (due to the experimental setup), the value of the diameter of the semi circle, i.e. the capacitance of the system, was unaffected by the noise.

Aptamers with longer linker type previously exhibited a 4-fold increase in binding capacity compared to those with shorter linkers[161]. Therefore, the surface chemistry based on the long linker DNA aptamer/EG did not show any sensitivity towards MPT64 nor specificity, hence, it was concluded not to use this surface chemistry for further MPT64 detection. As a result of both BioFET and EIS measurements, the surface chemistry based on the long linker DNA aptamer/MCH was chosen for further analysis.

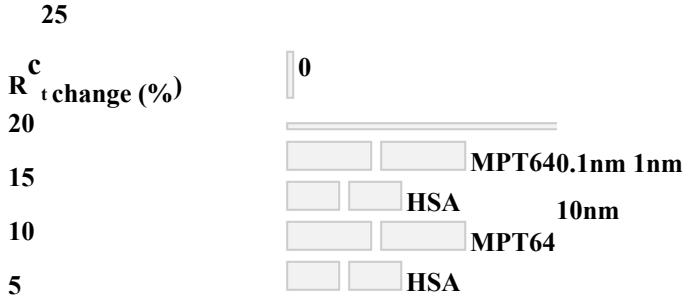

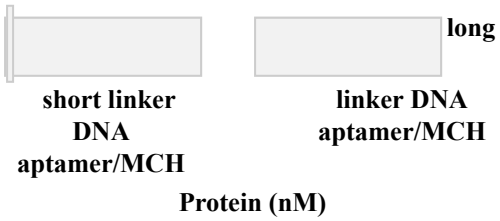

Figure 4.3 R_{ct} change for the electrode surface treated with a short linker-DNA aptamer/MCH and long linker DNA aptamer/MCH at a ratio of 1/100 followed by target incubation and measurement (in SELEX measurement buffer (50 mM Tris-HCl; 25 mM NaCl; 5 mM $MgCl_2$; pH 7.5) containing 2 mM ferro/ferricyanide $[Fe(CN)_6]^{3-/4-}$redox couple. Error bars show the mean and spread for at least three measurements from separate electrodes.

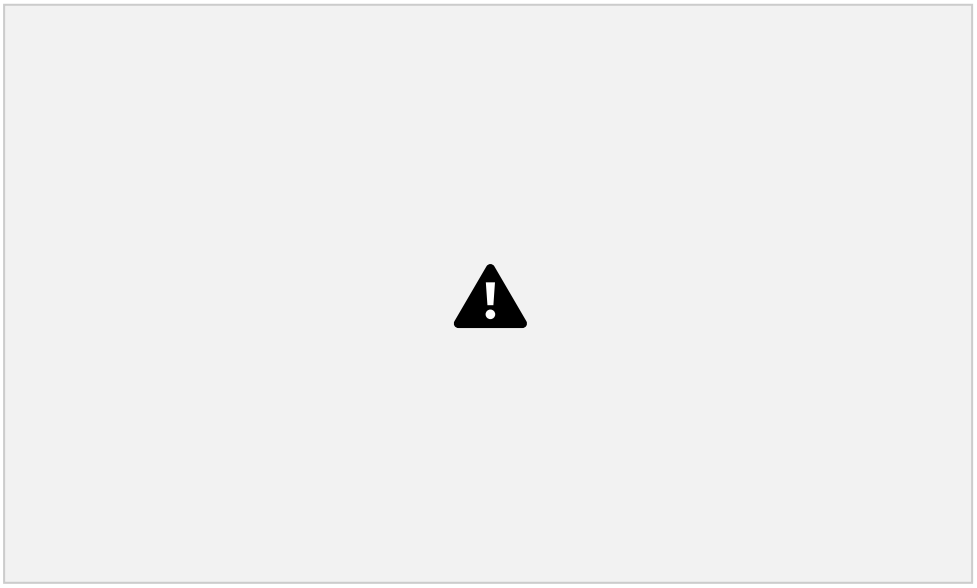

Figure 4.4 An example of non-Faradaic EIS measurement of the electrode modified long linker DNA aptamer/EG based surface chemistry upon MPT64 binding. Inset: original data.

4.3.2 Contact angle measurement

The contact angle measurement was used to validate each functionalization step in the aptasensor development and to demonstrate the binding between the target and modified surface. The contact angle was determined at different stages of the aptasensor development. **Figure 4.5 (**calculated values for three electrodes**)** and **Figure 4.6** (contact angle measurement

images for one electrode) presents different steps of aptasensor fabrication using aptamer/MCH ratio at 1/100. The images of each functionalization step was analyzed using the on screen protractor by placing the protractor at the base of each drop and consequent measurement of each angle corresponding to the shape of the drop. The measurement for each image was performed in the same way and the mean and spread for at least three measurements from separate electrodes was used to report the results. The surface of the electrode was hydrophilic for all measurements because of UV/ozone exposure during electrode surface preparation and cleaning steps. The contact angle of the bare gold electrode was 16.25° and an increase to 21.23° was observed after the MCH functionalization step. The contact angle value for the aptamer/MCH at 1/100 ratio was lower (20.45°) compared to MCH alone indicating on a successful immobilization of aptamers on the surface. The subsequent interaction with a 50 nM MPT64 significantly lowered the value of the contact angle down to 16.52^{o}, demonstrating a specific binding to immobilized aptamers compared to control protein, HSA (19.7°). A small non-specific binding of HSA to the MCH treated surface was also shown in previous studies[113]

[154 161]. However, the change for non-specific binding was much lower than for specific binding and could be attributed to noise. The statistically significant difference between the means of each functionalization step was determined using one-way analysis of variance with an established $P = 1.69 \times 10^{-12}$ which is below $P<0.05$ indicating that the statistical mean values are significantly different. The relatively small error bars served as an indicator for the accuracy of the measurement as well as for the repeatability of the process. In addition, measurements conducted using EIS also confirmed the difference in R_{ct} after electrode functionalization steps (**Figure 4.9b**).

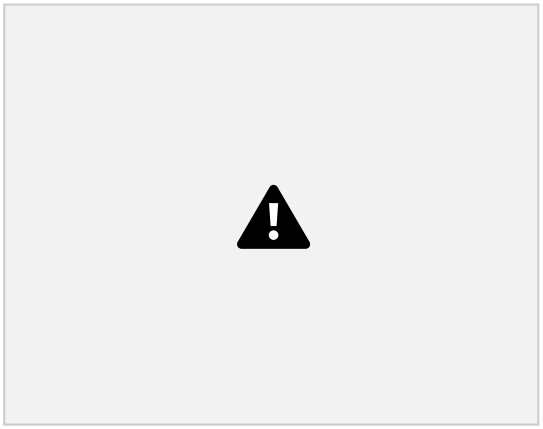

Figure 4.5 Contact angle measured on different steps of aptasensor fabrication using

aptamer/MCH ratio at 1/100. Error bars show the mean and spread for at least three measurements from separate electrodes.

4.3.3 Long linker DNA aptamer/MCH ratio optimization

The aptamer surface density on the gold electrode and aptamer geometry/positioning is extremely important for consequent target binding. Therefore, finding the best ratio of an aptamer and a co-adsorbent is essential for the aptasensor functionalization and development. Since the long linker aptamer/MCH complex based surface chemistry showed the highest signals, it was used further in the optimization analysis. A chronocoulometry method was used to determine the surface density of DNA aptamer[135] i.e. the best aptamer/MCH ratio for the optimal MPT64 binding. The method was based on the electrostatic interaction or intercalation of specific redox cations ($Ru(NH_3)_6^{3+}$) with the DNA's sugar-phosphate backbone. The amount of trapped redox marker at the DNA-modified electrode then determined using chronocoulometry. The surface density of the probe was calculated assuming complete charge compensation of the DNA phosphate residues by redox cations[165]. The long linker DNA aptamer

was co-immobilized with MCH onto the gold electrode, where the probe surface density was controlled by varying ratios of DNA aptamer and MCH in solution. A typical charge flow graph (**Figure 4.7a**) and chronocoulometric response curve (**Figure 4.7b**) with and without $Ru(NH_3)_6^{3+}$ for the long linker DNA aptamer/MCH at 1/100 ratio showed the difference in charge flow. The data from the graphs were used to determine the DNA aptamer density using the integrated Cottrell's equation[135].

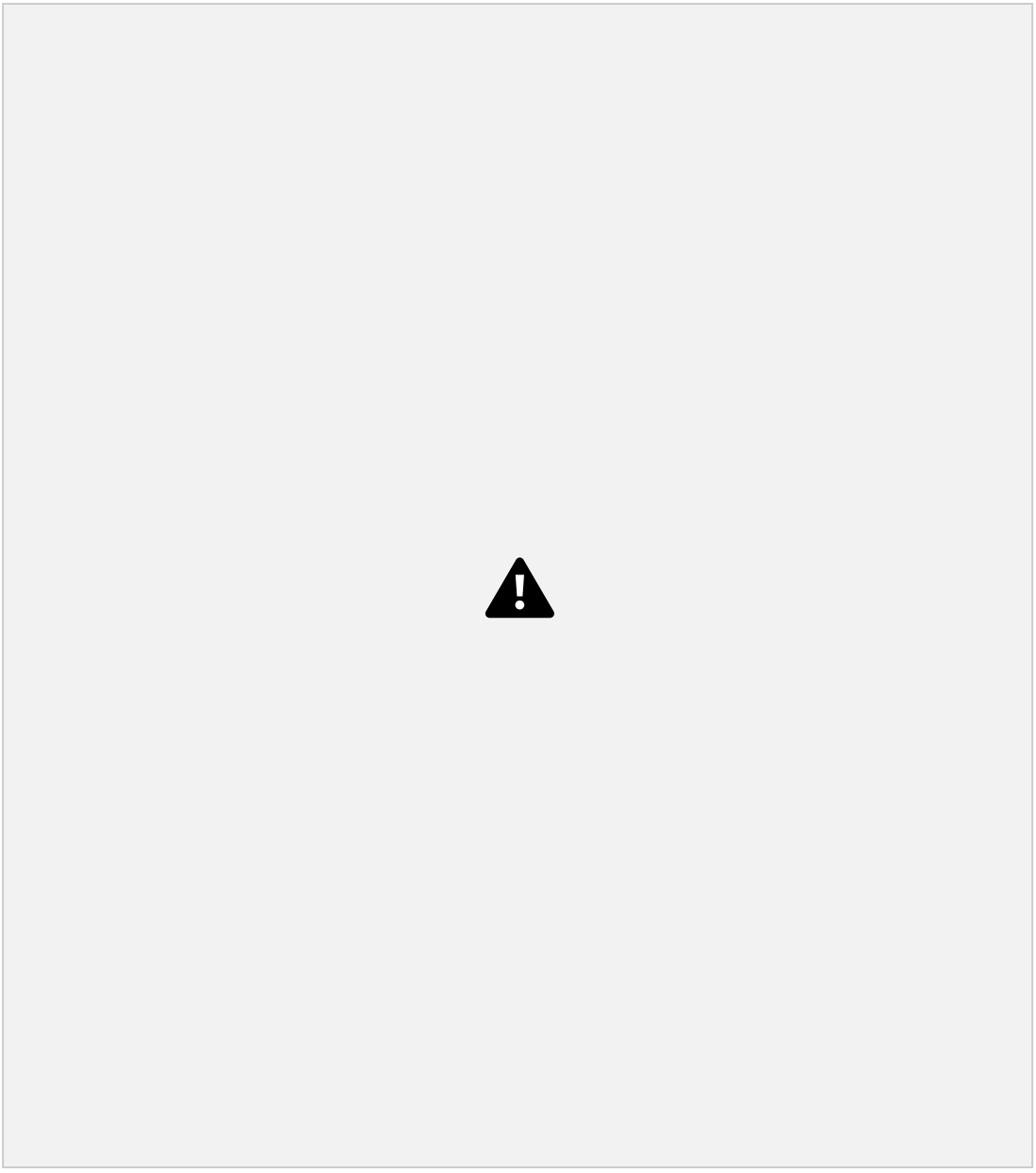

Figure 4.6 Contact angle measurement images of one electrode corresponding to **(a)** bare gold; **(b)** MCH; **(c)** MCH/aptamer; **(d)** MCH/aptamer MPT64; **(e)** MCH/aptamer HSA.

The variation of the surface density of the long linker DNA aptamer at different ratios of MCH is shown in **Figure 4.8a**, where four DNA aptamer/MCH ratios were tested: 1/50, 1/100, 1/200, and 1/500. The DNA aptamer density increased as the fraction of DNA to MCH increased from 6.50×10^{11} molecules/cm^{2}at 0.002% (1/50; aptamer/MCH) fraction of DNA up to 7.91×10^{11} molecules/cm^{2}at 0.02% (1/500; aptamer/MCH) DNA (**Table 4.1**). The aptasensor was further tested on target binding at three different MPT64 concentrations (0.1, 1, and 10 nM) by

impedance measurements and results were compared for different aptamer/MCH ratios (**Figure 4.8b**). By analyzing the R_{ct} change responses from the EIS signal, the four aptamers/MCH ratios showed different levels of R_{ct} change after incubating with MPT64. A significant increase in MPT64 binding was recorded at an aptamer/MCH ratio of 1/100 by the EIS compared to other ratios studied. For the determination of the same MPT64 concentration (e.g. 10nM MPT64), the difference of the change in R_{ct} signal (from 6 to 25%) using different ratios studied showed the signal increase in the order 1/500<1/50<1/200<1/100. A similar trend was also reported for aptasensors against prostate-specific antigen[164]. The 1/100 ratio with aptamer 7.66×10^{11} molecules/cm^{2}showed the highest R_{ct} shift: 3.0%, 10.4% and 24.7% upon MPT64 binding at concentrations 0.1, 1, and 10 nM, respectively. The next in line for improved sensitivity to MPT64 protein was aptamer/MCH ratio at 1/200 followed by 1/500 where the aptasensor could still detect MPT64 however with less binding due to the decreased number of aptamer molecules as well as increased sparsity between individual aptamers on the electrode surface. The 1/50 ratio showed lower R_{ct} change (0.01%, 1.6% and 11.6% at 0.1, 1, and 10 nM, respectively) compared to the 1/100 ratio, and it didn't follow the same trend as with the other ratios studied. This might indicate that the surface was too densely packed, which lowered the sensitivity towards the MPT64 at 1/50 ratio due to steric hindrance effects. Taking into consideration the long linker that was attached to the aptamer and the size of the aptamer itself, which was comparatively long (40 nucleotides), the densely packed surface disabled the aptamer from specific binding to the MPT64. This could be due to the fact that aptamer configuration did not have a freely moving brush-like confirmation or it was due to the charge effects from the DNA at 1/50 ratio. Since it is extremely important to find the balance which gives an optimal signal, a ratio of 1/100 was chosen for further aptasensor development.